Office of Naval Research

Contract N50RI-76 • Task Order No.1 • NR-078-011

THE RADIATION OF A HERTZIAN DIPOLE OVER A COATED CONDUCTOR

By

Donald B. Brick

May 10, 1953

Technical Report No. 172

Cruft Laboratory
Harvard University
Cambridge, Massachusetts

Office of Naval Research

Contract N5ori-76

Task Order No. 1

NR-078-011

Technical Report on The Radiation of a Hertzian Dipole over a Coated Conductor

by

Donald B. Brick

May 10, 1953

The research reported in this document was made possible through support extended Cruft Laboratory, Harvard University, jointly by the Navy Department (Office of Naval Research), the Signal Corps of the U. S. Army, and the U. S. Air Force under ONR Contract N5ori-76, T. O. 1.

Technical Report No. 172

Cruft Laboratory

Harvard University

Cambridge, Massachusetts

TR172

The Radiation of a Hertzian Dipole over a Coated Conductor

by

Donald B. Brick

Cruft Laboratory, Harvard University

Cambridge, Massachusetts

Abstract

The idealized problems of (a) an infinitesimal Hertzian dipole in and over a perfect dielectric coating a perfect conductor and (b) as Abraham dipole lying on the conductor are treated. Unintegrated forms of the Hertz potentials are obtained for both electric and magnetic dipoles.

Integrated far-zone forms of the potentials and fields are obtained for electric dipoles by means of asymptotic integrations. Far-zone radiation patterns are given in order to indicate the distortions of the fields and the magnitudes of the residue waves caused by the dielectric coatings.

It is proved that the power radiated by the dipole may be divided into two independent quantities-the power fed to radiation type and that fed to surface or guided type fields. For certain cases numerical results are given for the total power radiated and the relative powers fed to the two types of fields.

Formulas are derived and illustrated with numerical examples of the radiation resistances of the dipoles and the attenuation constants of the surface modes due to finite conductivity of the ground plane.

- - - - - - -

I.

Introduction

A study of the coated conductor problem was undertaken in an effort to explain certain characteristics of an antenna

field pattern obtained from measurements taken over an aluminum ground screen. The effect of the finite conductivity of the aluminum did not yield an adequate explanation of the observed characteristics near the ground screen and subsequent measurements showed that the phenomenon could be emphasized by the addition of a dielectric layer to the ground plane. Since a dielectric coated metallic surface can support a guided wave for any thickness of coating, it was deduced that the thin coating of aluminum oxide present on the ground screen was responsible for the behavior.

The idealized problem involves a uniform layer of perfect dielectric covering an infinite, perfectly-conducting plane; a Hertzian dipole is in one of three positions: Case A, above the dielectric; Case B, in the dielectric; or Case C, an Abraham dipole on the plane, Fig. I. Unintegrated expressions are derived for the Hertz potentials in and above the dielectric due to both vertical electric and magnetic dipoles. For the special cases of vertical electric dipoles in or near fairly thin dielectric coatings the integrated forms of the far-zone fields are obtained. Marcuvitz[1] has derived a similar expression for the Hertz potential above the dielectric due to a dipole above but near a thin dielectric coating by a somewhat different method. The mathematical details of this problem are similar to those of the vertical dipole over a conducting earth.[2,3]

The resulting fields, comprising a radiated-type wave (or compensating wave) and one or more guided-type waves, have been combined at typical distance for a polystyrene coating to yield field patterns. Several examples of these are given illustrating the distortion of the patterns due to dielectric layers. To further illustrate this distortion, expressions are derived for the total power output of the dipole, the ratio of the powers in the guided and radiated waves, and the radiation resistances of the dipoles. Where possible in the illustrative

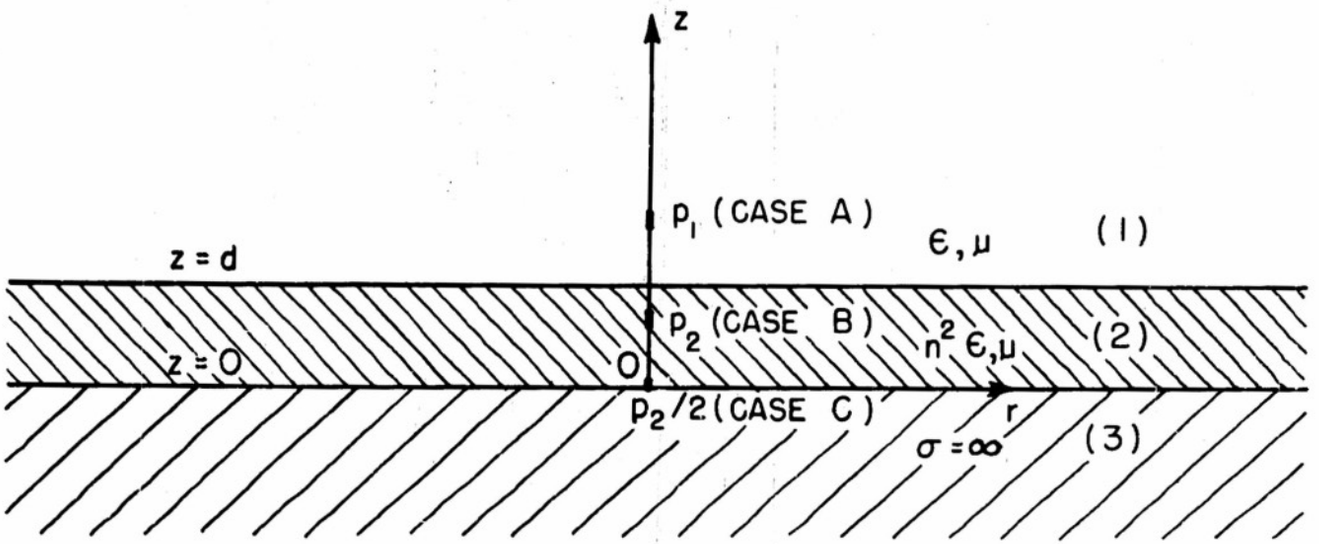

FIG. 1 CROSS-SECTION OF THE COATED PERFECT CONDUCTOR SHOWING THE COORDINATE SYSTEM USED

curves of these expressions, comparison curves for metal surfaces without dielectric coatings are given. In addition, the expression for the attenuation constants of the guided waves due to finite but large conductivities of the conducting plane is derived. No attempt is made at this time to compute the attenuation due to conductivity of the dielectric. A good approximation to this attenuation is given by Attwood.[4]

II

Formulation

Let an infinitesimal electric Hertzian dipole, a magnetic dipole, or an Abraham dipole be oriented along and parallel to the z-axis of the cylindrical coordinate system r, θ, z, Fig. I. This system is independent of θ. Region I, $d \leq z \leq \infty$, with constants ε, u, $\sigma = o$, is the space above the dielectric; region 2, with constants $n^2\varepsilon$, μ, $\sigma = o$, $o \leq z \leq d$, is the dielectric region; and region 3, $z \leq o$ is a perfect conductor with $\sigma = \infty$ The dielectric constant of medium 2 relative to that of medium 1 is n^2, where n is the index of refraction.

As is well known the electromagnetic field excited by electric or magnetic sources oriented in the z - direction of a cylindrical coordinate system may be derived from the z - components of the electric or magnetic Hertz vectors. Hence, the problem will be formulated in terms of these components.

The problem is subdivided into five divisions according to the positions of the dipoles and as to whether the electric or magnetic case is treated. The harmonic time dependence $e^{-i\omega t}$ is assumed throughout* and is cancelled in all expressions.

- - - - - - -

*To convert to dependence $e^{j\omega t}$ substitute j for -i.

Vertical Electric Dipoles

Case A A Hertzian dipole above the dielectric at $d \leq z' \leq \infty$, $r' = 0$.

$$1. \quad \nabla^2 \underset{(A)}{\pi_1} + \beta^2 \underset{(A)}{\pi_1} = -\frac{p_1(z')\delta(z-z')\delta(r)}{2\pi\varepsilon r} \qquad \text{Region 1}$$

$$2. \quad \nabla^2 \underset{(A)}{\pi_2} + n^2\beta^2 \underset{(A)}{\pi_2} = 0 \qquad \text{Region 2}$$

Case B A Hertzian dipole in the dielectric at $0 < z' \leq d$, $r' = 0$.

$$3. \quad \nabla^2 \underset{(B)}{\pi_1} + \beta^2 \underset{(B)}{\pi_1} = 0 \qquad \text{Region 1}$$

$$4. \quad \nabla^2 \underset{(B)}{\pi_2} + n^2\beta^2 \underset{(B)}{\pi_2} = -\frac{p_2(z')\delta(z-z')\delta(r)}{2\pi n^2 \varepsilon r} \qquad \text{Region 2}$$

Case C An Abraham dipole on the ground plane at $z' = 0$, $r' = 0$.

$$5. \quad \nabla^2 \underset{(C)}{\pi_1} + \beta^2 \underset{(C)}{\pi_1} = 0 \qquad \text{Region 1}$$

$$6. \quad \nabla^2 \underset{(C)}{\pi_1} + n^2\beta^2 \underset{(C)}{\pi_2} = -\frac{p_2(o)\delta(z)\delta(r)}{4\pi n^2 \varepsilon r} \qquad \text{Region 2}$$

The appropriate boundary conditions are:

$$7. \quad a) \qquad \frac{\partial \pi_1}{\partial z}(r,d,z') = \frac{\partial \pi_2}{\partial z}(r,d,z')$$

$$b) \qquad \varepsilon \pi_1(r,d,z',) = n^2 \varepsilon \pi_2(r,d,z')$$

c) $$\frac{\partial \pi_2}{\partial z}(r,o,z') = 0$$

d) The Sommerfeld condition of radiation,[5,6]

where:

$\pi_1(r,z,z')$ is the z-component of the electric Hertz vector in region 1.

$\pi_2(r,z,z')$ is the z-component of the electric Hertz vector in region 2.

These are defined by:

8. $$\begin{Bmatrix} \vec{E}_1 \\ \vec{E}_2 \end{Bmatrix} = \hat{r}\frac{\partial^2}{\partial r \partial z}\begin{Bmatrix} \pi_1 \\ \pi_2 \end{Bmatrix} + \hat{z}\left(\frac{\partial^2}{\partial z^2} + \beta^2 \begin{Bmatrix} 1 \\ n^2 \end{Bmatrix}\right)\begin{Bmatrix} \pi_1 \\ \pi_2 \end{Bmatrix}.$$

9. $$\begin{Bmatrix} \vec{B}_1 \\ \vec{B}_2 \end{Bmatrix} = \hat{\theta} i \frac{\beta^2}{\omega} \frac{\partial}{\partial r} \begin{Bmatrix} \pi_1 \\ n^2 \pi_2 \end{Bmatrix}$$

The upper quantities in the brackets are valid in region 1 and the lower quantities in region 2.

$\beta = \omega\sqrt{\varepsilon\mu}$

$m^2 =$ relative dielectric constant of region 2 with respect to region 1.

$\left.\begin{matrix} p_1(z') \\ p_2(z') \end{matrix}\right\}$ is a vertical Hertzian dipole at z' $\begin{cases} d \leq z' \leq \infty \\ 0 < z' \leq d \end{cases}$

$p_2(0)/2$ is an Abraham dipole at $z' = 0$

$\nabla^2 = \frac{1}{r}\frac{\partial}{\partial r}\left(r\frac{\partial}{\partial r}\right) + \frac{\partial^2}{\partial z^2} =$ The Laplacion operator in the cylindrical coordinate system with no θ dependance.

$\frac{\delta(z-z')\delta(r)}{2\pi r}$ is the Dirac delta-function for a source at $z = z'$, $r = 0$.

Vertical Magnetic Dipoles

Case A A magnetic dipole above the dielectric at $d \leq z' \leq \infty$, $r' = 0$

11. $\nabla^2 \pi_{m1}^{(A)} + \beta^2 \pi_{m1}^{(A)} = - \frac{\mu m_1(z')\delta(z-z')\delta(r)}{2\pi r}$ Region 1

12. $\nabla^2 \pi_{m2}^{(A)} + n^2\beta^2 \pi_{m2}^{(A)} = 0$ Region 2

Case B A magnetic dipole in the dielectric at $0 < z' \leq d$, $r' = 0$

13. $\nabla^2 \pi_{m1}^{(B)} + \beta^2 \pi_{m1}^{(B)} = 0$ Region 1

14. $\nabla^2 \pi_{m2}^{(B)} + n^2\beta^2 \pi_{m2}^{(B)} = - \frac{\mu m_2(z')\delta(z-z')\delta(r)}{2\pi r}$ Region 2

One should note that the problem of a magnetic dipole placed at $z' = 0$ need not be formulated since according to the theory of images it yields fields which are identically zero.

The appropriate boundary conditions are

15. a) $\pi_{m1}(r,d,z') = \pi_{m2}(r,d,z')$

b) $\frac{\partial}{\partial z} \pi_{m1}(r,d,z') = \frac{\partial}{\partial z} \pi_{m2}(r,d,z)$

subject to $\mu_1 = \mu_2 = \mu$

c) $\pi_{m2}(r,o,z') = 0$

d) The radiation condition.[5,6]

Where:

$$\left.\begin{matrix}\pi_{m1}(r,z,z') \\ \pi_{m2}(r,z,z')\end{matrix}\right\}$$ is the z-component of the magnetic Hertz vector in $\begin{cases}\text{region 1}\\ \text{region 2}\end{cases}$

These are defined by:

16. $$\begin{Bmatrix}\vec{E}_{1m}\\ \vec{E}_{2m}\end{Bmatrix} = -i\omega\hat{\theta}\frac{\partial}{\partial r}\begin{Bmatrix}\pi_{m1}\\ \pi_{m2}\end{Bmatrix}$$

17. $$\begin{Bmatrix}\vec{B}_{1m}\\ \vec{B}_{m2}\end{Bmatrix} = \hat{z}\left(\frac{\partial^2}{\partial z^2} + \beta^2\begin{Bmatrix}1\\ n^2\end{Bmatrix}\right)\begin{Bmatrix}\pi_{m1}\\ \pi_{m2}\end{Bmatrix} + \hat{r}\frac{\partial^2}{\partial r\partial z}\begin{Bmatrix}\pi_{m1}\\ \pi_{m2}\end{Bmatrix}$$

Where the subscript m indicates quantities in the magnetic cases and

$$\left.\begin{matrix}m_1(z')\\ m_2(z')\end{matrix}\right\}$$ is a vertical magnetic dipole at $z'\begin{cases}d\le z'\le\infty\\ o<z'\le d\end{cases}$

Since the problem is formulated in cylindrical coordinates with θ - symmetry it is convenient to apply the well-known Fourier - Bessel or Hankel Transform pair[7] for θ symmetry to equations 1-6 and 11-14.

18. $$\bar{\pi}(\lambda,z,z') = \int_o^\infty r\pi(r,z,z')J_o(\lambda r)dr$$

19. $$\pi(r,z,z') = \int_o^\infty \lambda\bar{\pi}(\lambda,z,z')J_o(\lambda r)d\lambda$$

After applying equation 18 to the equations 1-6 and 11-14, performing an integration by parts, and applying the radiation condition* to the left sides of these equations the following

* The quantity $\left[\frac{\partial\pi}{\partial r}rJo(\lambda r) - \pi r\lambda J_1(\lambda r)\right]_o$ appears after the integration by parts. This disappears identically at r=o and at r = ∞ the radiation condition 5.6 requires its disappearance.

results are obtained for the left sides of these equations:

for equations 1, 3, 5, 11, 13

$$\left(\frac{\partial^2}{\partial z^2} - \ell^2\right) \bar{\pi}_1 \text{ or } m_1$$

for equations 2, 4, 6, 12, and 14

$$\left(\frac{\partial^2}{\partial z^2} - m^2\right) \bar{\pi}_2 \text{ or } m_2$$

where ℓ^2 and m^2 are defined:

20. $$\ell^2 = \lambda^2 - \beta^2$$

21. $$m^2 = \lambda^2 - n^2\beta^2$$

After noting that the application of equation 18 to the right sides of equations 1, 4, 6, 11 and 14 yields the value $1/2\pi$, the following transformed equations are obtained:

22.
$$\left(\frac{\partial^2}{\partial z^2} - \ell^2\right) \left\{ \begin{array}{lcl} \bar{\pi}_{1(A)} & = & -\dfrac{p_1(z')\delta(z-z')}{2\pi\varepsilon} \\ \bar{\pi}_{1(B)} & = & 0 \\ \bar{\pi}_{1(C)} & = & 0 \\ \bar{\pi}_{m1(A)} & = & -\dfrac{\mu m_1(z')\delta(z-z')}{2\pi} \\ \bar{\pi}_{m1(B)} & = & 0 \end{array} \right\}$$

23.
$$\left(\frac{\partial^2}{\partial z^2} - m^2\right)\left\{\begin{array}{lll} \bar{\pi}_{2(A)} & = & 0 \\ \bar{\pi}_{2(B)} & = & -\dfrac{p_2(z')\delta(z-z')}{2\bar{\pi}n^2\varepsilon} \\ \bar{\pi}_{2(C)} & = & -\dfrac{p_2(0)\delta(z)}{4\bar{\pi}n^2\varepsilon} \\ \bar{\pi}_{m2(A)} & = & 0 \\ \bar{\pi}_{m2} & = & -\dfrac{\mu m_2(z')\delta(z-z')}{2\bar{\pi}} \end{array}\right\}$$

These are the transformed forms of equations 1, 3, 5, 11, 13 and 2, 4, 6, 12, and 14 respectively. These satisfy boundary conditions 7 a-d and 15 a-d as can be seen from equations 18 and 19 assuming that the order of integration and differentiation, with respect to z, may be interchanged.

According to the physical considerations of these problems it is convenient to substitute the following forms in equations 22 and 23. If these satisfy the equations and boundary conditions they are the unique solutions of the problems except for an arbitrary constant in time.[8] The subscripts indicate the equation to which each trial solution belongs.

24.
$$\left.\begin{array}{l} \dfrac{\varepsilon\bar{\pi}_1(\lambda,z,z')}{p_1(z')} \\ \\ \dfrac{\bar{\pi}_{m1}(\lambda,z,z')}{\mu m_1(z')} \end{array}\right\} = \frac{1}{4\bar{\pi}\ell}\, e^{-\ell|z-z'|} + B(\lambda,z')\, e^{-\ell(z+z'-2d)}e^{+2md} + C(\lambda,z')e^{-\ell(z+z'-2d)}$$

Where the first term is the incident wave or the wave radiated by an isolated source, the second term is a wave reflected from the metal surface, and the third term represents a wave reflected

from the dielectric surface.

$$25.\quad \left.\begin{array}{l} \dfrac{\varepsilon\bar{\pi}_2(\lambda,z,z')}{\underset{(A)}{p_1(z')}} \\ \\ \dfrac{\bar{\pi}_{m2}(\lambda,z,z')}{\underset{(A)}{\mu m_1(z')}} \end{array}\right\} = D(\lambda,z')\,e^{-[\ell|d-z'| + m(d-z)]} + E(\lambda,z')\,e^{-[\ell|d-z'| + m(d+z)]}$$

Where the first term is a wave transmitted into the dielectric and the second term is a wave reflected from the metal surface.

$$26.\quad \left.\begin{array}{l} \dfrac{n^2\varepsilon\bar{\pi}_2(\lambda,z,z')}{\underset{(B)}{p_2(z')}} \\ \\ \dfrac{2n^2\varepsilon\bar{\pi}_2(\lambda,z,0)}{\underset{(C)}{p_2(0)}} \\ \\ \dfrac{\bar{\pi}_{m2}(\lambda,z,z')}{\underset{(B)}{\mu m_2(z')}} \end{array}\right\} = \frac{1}{4\pi m}\,e^{-m|z-z'|} + F(\lambda,z')\,e^{-m(2d-z-z')} + G(\lambda,z')\,e^{-m(z+z')}$$

$z' = 0$ for case C.

Where the first term is the incident wave, the second term is a wave reflected from the boundary $z = d$, and the third term is a wave reflected from the metal boundary.

$$27.\quad \left.\begin{array}{l} \dfrac{n^2 \varepsilon \bar{\pi}_1(\lambda,z,z')}{\underset{(B)}{p_2(z')}} \\[2ex] \dfrac{2n^2 \varepsilon \bar{\pi}_1(\lambda,z,o)}{\underset{(C)}{p_2(0)}} \\[2ex] \dfrac{\bar{\pi}_{m1}(\lambda,z,z')}{\underset{(B)}{\mu m_2(z')}} \end{array}\right\} = H(\lambda,z')e^{-\lambda(z-d)},$$

where this term represents a wave radiated from the dielectric surface.

It may be observed that the left sides of equations (24-27) are the Green's functions for equations (22-23). The proper choice of the coefficients of the first terms on the right sides of equations (24) and (26) gaurantees that these equations satisfy the conditions for the Greens functions at $z = z'$.

Substituting equations equations (24-27) in their proper boundary conditions 7a-d or 15a-d, it may be verified that the trial solutions 24-27 indeed do satisfy the boundary conditions. Evaluating the constants $B(\lambda,z')$ through $H(\lambda,z')$ yields the transformed Hertz potentials. Applying the Fourier-Bessel integral, 19, rearranging the resulting integrals, and using equation (28),[9] yield the Hertz potentials, 29-38, which are the solutions to equations (1-6) and (11-14).

$$28.\quad \frac{1}{4\pi}\int_0^\infty \frac{J_o(\lambda r)\, e^{-|z|\sqrt{\lambda^2-k^2}}}{\sqrt{\lambda^2-k^2}}\,\lambda d\lambda = \frac{e^{ik\sqrt{r^2+z^2}}}{4\pi\sqrt{r^2+z^2}}$$

Vertical Electric Dipoles

Case A

29. $$\pi_{1(A)}(r,z,z') = \frac{p_1(z')}{4\pi\varepsilon}\left[\frac{e^{i\beta R'}}{R'} - \frac{e^{i\beta R''}}{R''} + 2\int_0^\infty \frac{\cosh md\, e^{-\ell(z+z'-2d)}}{M(\beta,\lambda,n,d)}\lambda Jo(\lambda r)d\lambda\right]$$

Region 1

30. $$\pi_{2(A)}(r,z,z') = \frac{p_1(z')}{2\pi\varepsilon n^2}\int_0^\infty \frac{\cosh mz\, e^{-\ell(z'-d)}}{M(\beta,\lambda,n,d)}\lambda Jo(\lambda r)d\lambda$$

Region 2

Case B

31. $$\pi_{1(B)}(r,z,z') = \pi_{2(A)}(r,z',z)\frac{p_2(z')}{p_1(z')} = \frac{p_2(z')}{2\pi\varepsilon m^2}\int_0^\infty \frac{\cosh mz'\, e^{-\ell(z-d)}}{M(\beta,\lambda,n,d)}\lambda Jo(\lambda r)d\lambda$$

Region 1

32. $$\pi_{2(B)}(r,z,z') = \frac{p_2(z')}{4\pi n^2\varepsilon}\left[\frac{e^{in\beta R'}}{R'} + \frac{e^{in\beta R^V}}{R^V} - 2\int_0^\infty \frac{(\ell - m/n^2)\cosh mz'\cosh mz\, e^{-md}}{m\, M(\beta,\lambda,n,d)}\lambda Jo(\lambda r)d\lambda\right]$$

Region 2

Case C

33. $$\pi_{1(C)}(r,z,0) = \frac{p_2(0)}{4\pi\varepsilon n^2}\int_0^\infty \frac{e^{-\ell(z-d)}}{M(\beta,\lambda,n,d)}\lambda Jo(\lambda r)d\lambda$$

Region 1

$$34.\quad \underset{(C)}{\pi_2}(r,z,0) = \frac{p_2(0)}{4\pi n^2\varepsilon}\left[\frac{e^{in\beta R}}{R} - \int_0^\infty \frac{(\ell - m/n^2)\cosh mz\, e^{-md}\lambda J_0(\lambda r)d\lambda}{m\, M(\beta,\lambda,n,d)}\right]$$

Region 2

Vertical Magnetic Dipoles

Case A

$$35.\quad \underset{(A)}{\pi_{m1}}(r,z,z') = \frac{\mu m_1(z')}{4\pi}\left[\frac{e^{i\beta R'}}{R'} - \frac{e^{i\beta R''}}{R''} + 2\int_0^\infty \frac{\sinh md}{N(\beta,\lambda,n,d)}\, e^{-\ell(z+z'-2d)}\lambda J_0(\lambda r)d\lambda\right]$$

Region 1

$$36.\quad \underset{(A)}{\pi_{m2}}(r,z,z') = \frac{\mu m_1(z')}{2\pi}\int_0^\infty \frac{\sinh mz}{N(\beta,\lambda,nd)}\, e^{-\ell(z'-d)}\lambda J_0(\lambda r)d\lambda$$

Region 2

Case B

$$37.\quad \underset{(B)}{\pi_{m1}}(r,z,z') = \underset{(A)}{\pi_{m2}}(r,z'z)\frac{m_2(z')}{m_1(z')}$$

$$= \frac{\mu m_2(z')}{2\pi}\int_0^\infty \frac{\sinh mz'}{N(\beta,\lambda,n,d)}\, e^{-\ell(z-d)}\lambda J_0(\lambda r)d\lambda$$

Region 1

$$38.\quad \underset{}{\pi_{m2}}(r,z,z') = \frac{\mu m_2(z')}{4\pi}\left[e\frac{i\beta R'}{R'} - e\frac{i\beta R^V}{R^V} - 2\int_0^\infty \frac{(\ell - m)\sinh mz'\sinh mz}{mN(\beta,\lambda,n,d)}\, e^{-md}\lambda J_0(\lambda r)d\lambda\right]$$

Region 2

Where

$$39.\quad M(\beta,\lambda,n,d) = \ell\cosh md + \frac{m}{n^2}\sinh md$$

$$40.\quad N(\beta,\lambda,n,d) = \ell\sinh md + m\cosh md.$$

R is the spherical coordinate distance of Figs. 2a and 2c.

$$= \sqrt{r^2 + z^2}$$

$$R' = \sqrt{r^2 + (z-z')^2} \qquad \text{Fig. 2a}$$

$$R'' = \sqrt{r^2 + (z+z'-2d)^2} \qquad \text{Fig. 2a}$$

$$R^V = \sqrt{r^2 + (z+z')^2}$$

It is to be observed in equations 29-38 that the forms of the integrands of the unintegrated terms indicate that these are standing wave distributions or multiple reflections of the waves from the dielectric and metal surface in region 2, the dielectric region. The integrated terms indicate that the dipoles are imaged in the dielectric or metal surface.

The E and B fields may be derived through the application of equations 8 and 9 or 16 and 17.

III

Far-Zone Formulations of the Hertz Potentials

The Hertz potentials π_1 and π_2 for vertical electric dipoles are asymptotically integrated to obtain far-zone expressions with the restriction of thin dielectric coatings. The integrations of equations 2.29-2.31 and equation 2.33, Appendix A, are similar to those performed by Tai[10] and others.[11,12] Equations 2.32 and 2.34 are integrated using the method of Van Der Waerden,[13] Appendix B.

The integrals in equations 2.29-2.34 are transformed to a symmetric form for $r > o$:

$$(1) \qquad \int_o^\infty F(\lambda) J_o(\lambda r) \lambda d\lambda = \frac{1}{2} \int_{-\infty}^{\infty} F(\lambda) H_o^1(\lambda r) \lambda d\lambda$$

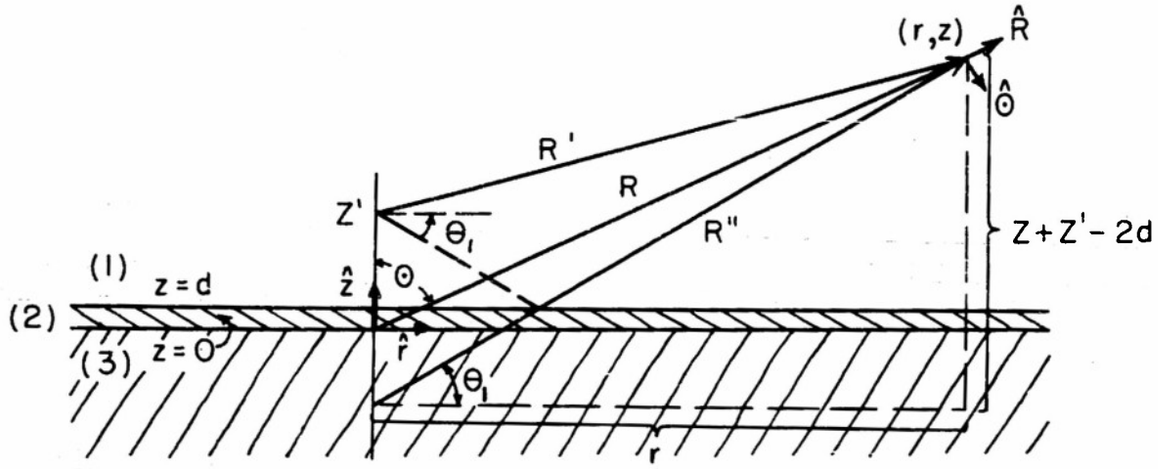

FIG. 2a COORDINATES FOR CASE A—1

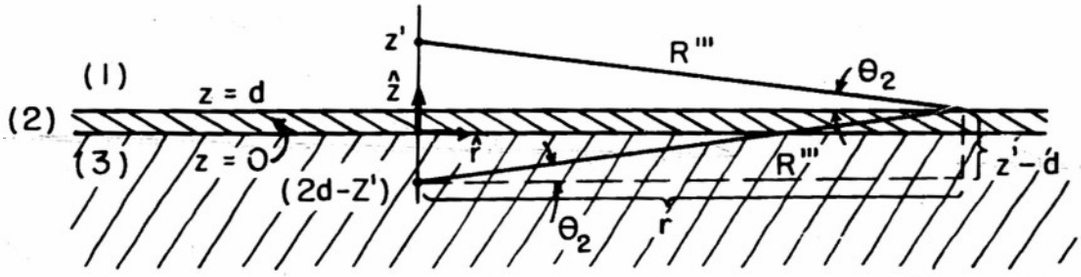

FIG. 2b COORDINATES FOR CASE A—2

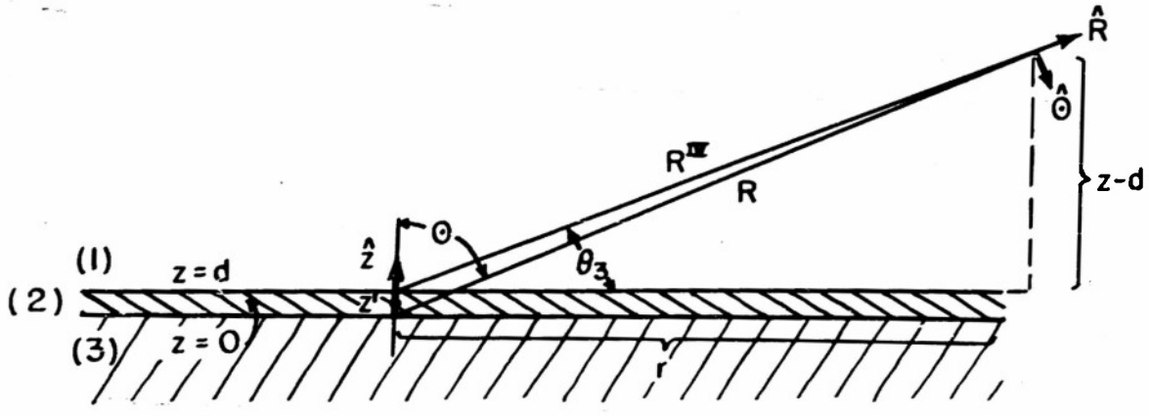

FIG. 2c COORDINATE FOR CASE B-1 AND C-1

through the use of:[14]

$$J_o(\lambda r) = \frac{1}{2}\left[H_o^{1}(\lambda r) + H_o^{2}(\lambda r)\right]$$

and

$$H_o^{2}(\lambda r) = - H_o^{1}(-\lambda r)$$

where:

$F(\lambda)$ is an even function of λ, and $H_o^{1}(\lambda r)$ is chosen in order to yield outward travelling waves for real positive λ.

The integrands in equations 2.29 - 2.34 have first-order poles where $M(\beta,\lambda,n,d) = 0$, equation 2.39, or for solutions of:

$$(2) \qquad \pm n^2 \sqrt{\lambda^2-\beta^2} = \pm \sqrt{n^2\beta^2-\lambda^2}\, \tan\left(d\sqrt{n^2\beta^2-\lambda^2}\right)$$

Examining equation (2) in the light of equations 2.29 - 2.31, it is found that ℓ and m must be either positive real or negative imaginary numbers in order not to violate the radiation condition.[5,6] It is also observed that solutions exist only for the same sign on both sides of equation 2 and that the roots must satisfy:

$$(3) \qquad \beta \leq \lambda_J \leq n\beta$$

Figure 4 contains curves of λ_J/β versus βd, the electrical dielectric thickness, for $n^2 = 2.54$, polystyrene, and for $n^2 = 2.25$, polystyrene, in the range $.10\pi \leq \beta d \leq 1.6\pi$. Equation 2 has at least one solution for all βd, $\beta d > 0$. A new solution or root λ_k appears when:

$$(4) \qquad \beta d = \frac{k\pi}{\sqrt{n^2-1}} \quad k = 0,1,2, \ldots n .$$

Henceforth k will designate the number of solutions of equation 2 for a given βd.

The integrands in equations 2.29 - 2.31 and 2.33 have branch points of $\ell = 0$ or $\lambda = \pm \beta$, (1) and (2) in Fig. 3, and at $\lambda = 0$, (5) in Fig. 3, and poles at $\lambda = \lambda_1, \ldots, \lambda_k$. Upon examination of the integrals for slightly complex β and n,

it is seen that the integrals are to be taken over path W_1 in the complex λ plane of Fig. 3.

The integrands in equations 2.32 and 2.34 have additional branch points at $m = 0$, $\lambda = \pm n\beta$, (3) and (4) in Fig. 3, and in addition the same poles and branch points as the former integrands. These integrals are to be taken over W_2.

The evaluation of the k residues and the combination of these with the assymptotic integrations, performed in Appendices A and B, yield the far-zone Hertz potentials, equations 5 - 10, subject to:

$$\beta R >> \left\{ \begin{matrix} 1 \\ \text{and} \\ \beta d \end{matrix} \right\} \text{ where } R = \sqrt{r^2 + z^2}$$

and

$$e^{-R\left|\beta - \lambda_1\right|} << O(R^{-2}) << O(R^{-1})$$

$$e^{-R\left|n\beta - \lambda k\right|} << O(R^{-2}) << O(R^{-1})$$

or in other words the poles are not too near the branch points.

The terms in the summations in equations 5 - 10 which are due to the evaluation of the residues, are waves which propagate radially and attenuate exponentially in the z direction. These waves "hug" the surface and are hence called guided or surface waves. They result as eigenfunctions of the configuration, Fig. I, (excluding $r = 0$).[4, 16] The remaining terms will be designated as the radiating or compensating waves.

The far-zone Hertz potentials are:

Case A Hertz dipole above the dielectric at $d \le z' \le \infty$, $r' = 0$

$$5. \quad \underset{(A)}{\pi_1 F}(r,z,z') = \frac{p_1(z')}{\varepsilon} \left\{ \frac{e^{i\beta R'}}{4\pi R'} - \frac{e^{i\beta R''}}{4\pi R''} + \frac{P(\theta_1)}{R''} e^{i\beta R''} + \sum_{J=1}^{k} \frac{A_J(\theta_1) Q(\lambda_J, \beta, n, d)}{\sqrt{2\pi\lambda_J r}} e^{\left[i\lambda_J r - (z+z'-2d)\sqrt{\lambda_J^2 - \beta^2}\right]} \right\}$$

$$d \le z \le \infty$$

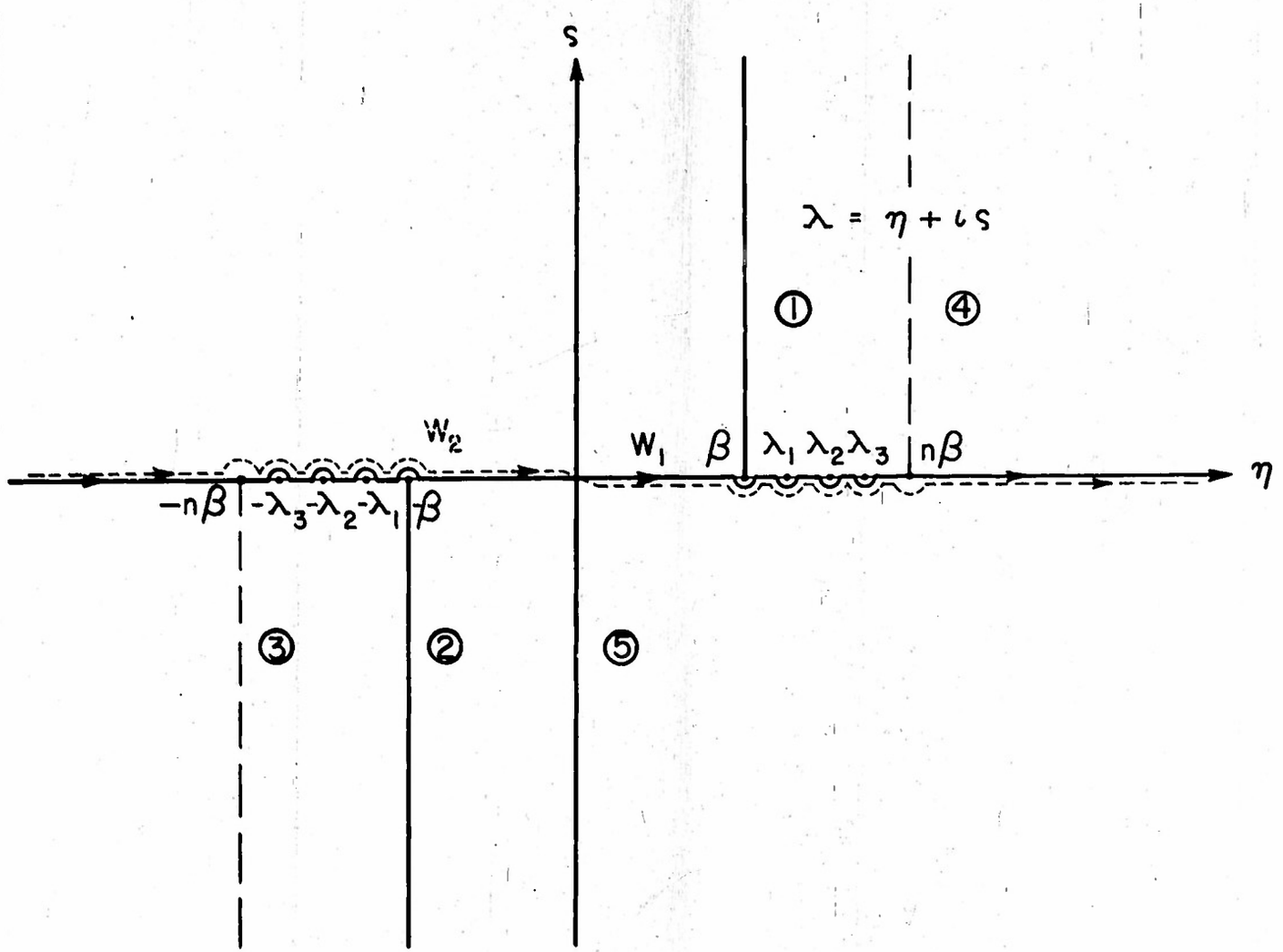

FIG. 3 PATHS OF INTEGRATION IN THE $\lambda = \eta + \iota s$ PLANE

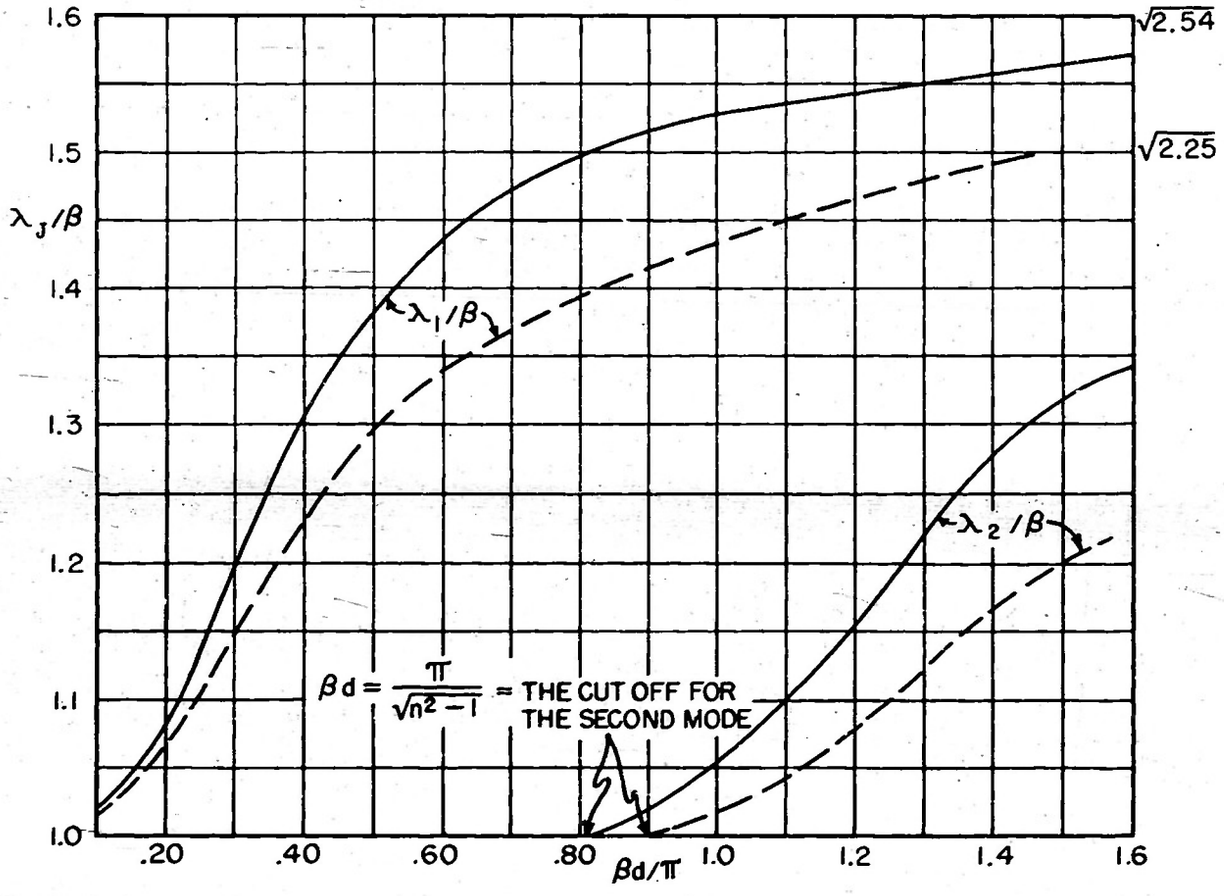

FIG. 4 λ_J/β VS. βd, FOR $n^2 = 2.54$ AND 2.25, $0.10\pi \leq \beta d \leq 1.6\pi$
$n^2 = 2.54$ ————, $n^2 = 2.25$ — — — —

$$6.\quad \underset{(A)}{\pi_2^F}(r,z,z') = \frac{p_1(z')}{n^2\varepsilon}\left\{\frac{P(\theta_2)\cos(\beta z\sqrt{n^2-\cos^2\theta_2})}{R'''\cos(\beta d\sqrt{n^2-\cos^2\theta_2})}\, e^{i\beta R'''}\right.$$

$$\left. + \sum_{J=1}^{k} \frac{A_J(\theta_2)Q(\lambda_J,\beta,n,d)\cos(z\sqrt{n^2\beta^2-\lambda_J^2})}{\sqrt{2\pi\lambda_J r}\cos(d\sqrt{n^2\beta^2-\lambda_J^2})}\, e^{[i\lambda_J r-(z'-d)\sqrt{\lambda_J^2-\beta^2}]}\right\}$$

$$0 \le z \le d$$

Case B Hertz dipole in the dielectric at $0 \le z \le d$, $r' = 0$

$$7.\quad \underset{(B)}{\pi_1^F}(r,z,z') = \frac{p_2(z')}{n^2\varepsilon}\left\{\frac{P(\theta_3)\cos(\beta z'\sqrt{n^2-\cos^2\theta_3})}{R^{IV}\cos(\beta d\sqrt{n^2-\cos^2\theta_3})}\, e^{i\beta R^{IV}}\right.$$

$$\left. + \sum_{J=1}^{k} \frac{A_J(\theta_3)Q(\lambda_J,\beta,n,d)\cos(z'\sqrt{n^2\beta^2-\lambda_J^2})}{\sqrt{2\pi\lambda_J r}\cos(d\sqrt{n^2\beta^2-\lambda_J^2})}\, e^{[i\lambda_J r-(z-d)\sqrt{\lambda_J^2-\beta^2}]}\right\}$$

$$d \le z \le \infty$$

$$8.\quad \underset{(B)}{\pi_2^F}(r,z,z') = \frac{p_2(z')}{\varepsilon n^4}\cdot$$

$$\sum_{J=1}^{k} \frac{Q(\lambda_J,\beta,n,d)\cos(z'\sqrt{n^2\beta^2-\lambda_J^2})\cos(z\sqrt{n^2\beta^2-\lambda_J^2})}{\sqrt{2\pi\lambda_J r}\cos^2(d\sqrt{n^2\beta^2-\lambda_J^2})}\, e^{i\lambda_J r}$$

$$0 \le z \le d$$

Case C Abraham dipole on the metal surface at $z' = 0$, $r' = 0$.

$$9.\quad \underset{(C)}{\pi_1^F}(r,z,0) = \frac{p_2(0)}{2n^2\varepsilon}\left\{\frac{P(\theta_3)\, e^{i\beta R^{IV}}}{R^{IV}\cos(\beta d\sqrt{n^2-\cos^2\theta_3})}\right.$$

$$\left. + \sum_{J=1}^{k} \frac{A_J(\theta_3)Q(\lambda_J,\beta,n,d)}{\sqrt{2\pi\lambda_J r}\cos(d\sqrt{n^2\beta^2-\lambda_J^2})}\, e^{(i\lambda_J r-(z-d)\sqrt{\lambda_J^2-\beta^2})}\right\}$$

$$d \le z \le \infty$$

$$10.\quad \pi_2^{(C)} F(r,z,0) = \frac{P_2(0)}{2n^4\varepsilon} \sum_{J=1}^{k} \frac{Q(\lambda_J,\beta,n,d)\cos(z\sqrt{n^2\beta^2-\lambda_J^2})}{\sqrt{2\pi\lambda_J r}\ \cos^2(d\sqrt{n^2\beta^2-\lambda_J^2})}\, e^{i\lambda_J r}$$

$$0 \le z \le d$$

Where:

$$P(\theta) = \frac{i\sin\theta}{2\pi[i\sin\theta + n^{-2}\sqrt{n^2-\cos^2\theta}\ \tan(\beta d\sqrt{n^2-\cos^2\theta})]}$$

$$Q(\lambda_J,\beta,n,d) = \frac{e^{i\pi/4}\sqrt{\lambda_J^2-\beta^2}\ (n^2\beta^2-\lambda_J^2)}{\beta^2(n^2-1) + d\sqrt{\lambda_J^2\beta^2}[n^2(\lambda_J^2-\beta^2)+(\beta^2-\lambda_J^2 n^{-2})]}$$

and $A_J(\theta)$ is defined by:

$$A_J(\theta) = 0 \quad \theta > \cos^{-1}\beta/\lambda_J$$

$$A_J(\theta) = \tfrac{1}{2} \quad \theta = \cos^{-1}\beta/\lambda_J$$

$$A_J(\theta) = 1 \quad \theta < \cos^{-1}\beta/\lambda_J$$

and

$$\theta_1 = \sin^{-1}\frac{z+z'-2d}{R''} = \cos^{-1} r/R''$$

$$R'' = \sqrt{r^2+(z+z'-2d)^2} \qquad \text{Fig. 2a}$$

$$\theta_2 = \sin^{-1}\frac{(z-d)}{R'''} = \cos^{-1} r/R'''$$

$$R''' = \sqrt{r^2+(z'-d)^2} \qquad \text{Fig. 2b}$$

$$\theta_3 = \sin^{-1}\frac{(z-d)}{R^{IV}} = \cos^{-1}\frac{r}{R^{IV}}$$

$$R^{IV} = \sqrt{r^2+(z-d)^2} \qquad \text{Fig. 2c}$$

If it is assumed that $\beta z' << \beta R'''$, the first term in 6 vanishes and $A_J(\theta_2) \equiv 1$.

The magnitudes of the fields of the guided modes attenuate with height z in two ways - first, the exponential or guiding factor $\exp(-z\sqrt{\lambda_J^2-\beta^2})$; second, the coefficient $A_J(\theta)$. The second factor is a function of βr while the first factor does not depend upon the radius. It may be observed that as βr increases the exponential attenuation takes precedence over the coefficient's attenuation. Fig. 5 contains curves of the minimum radii βr, for each mode, at which the field attenuates to 1 percent of its maximum value due to exponential attenuation, at a height βz less than that at which the coefficient $A_J(\theta)$ equals its critical value. These βr are plotted versus βd, in the range $.10\pi \leq \beta d \leq 1.6\pi$ and for $n^2 = 2.54$ and 2.25. For βr greater than these values $A_J(\theta) \equiv 1$ to within 1 percent accuracy.

The presence of the factor $A_J(\theta)$ indicates that as βr increases the guided wave acquires more power until at $\beta r = \infty$ the total power alloted to it has been attained. Making the assumption that $A_J(\theta)$ is identically one, for βr greater than the values of Fig. 5, is the same as assuming that the guided wave has acquired its total power at this βr. It is valid to within .01 percent accuracy with respect to the Poynting vector.

Since in this report the far fields are being investigated, it will be assumed henceforth that $\beta r(=\beta R \sin\theta)$ is greater than the values of Fig. 5 for each βd being investigated. For this reason the notation $A_J(\theta)$ will be dropped under the assumption that $A_J(\theta) \equiv 1$.

It is to be observed that, in order for the fields to be identical for sources at $z' = d+$ and $z' = d-$, $p_1(d+)=p_2(d-)/n^2$.

IV

The Far-Zone E- and B- Fields

The representation of the far-zone E- and B- fields are obtained by applying equations 2.8 and 2.9 to equations 3.5 - 3.10. Terms of order higher than r^{-1} are neglected. The assumption is made that $\beta z' << \beta R$ so that the radiation term in equation 3.6 may be neglected.

It is convenient to represent the radiating terms in spherical coordinates. The following substitutions[15] are made in the radiating waves assuming $\beta R >> 1$ in Fig. 2.

In the phase factors:

$$\beta R' = \beta R - \beta z' \cos\theta \qquad \beta R'' = \beta R - \beta(2d - z')\cos\theta$$

$$\beta R^{IV} = \beta R - \beta d \cos\theta$$

In the amplitude factors:

$$r/R'' = \cos\theta_1 \doteq \sin\theta = r/R \doteq r/R'$$

$$\frac{z + z' - 2d}{R''} = \sin\theta_1 \doteq \cos\theta = z/R \doteq (z - z')/R'$$

$$\beta R' \doteq \beta R'' \doteq \beta R$$

$$\sin\theta_3 = r/R^{IV} \doteq r/R = \cos\theta$$

$$\cos\theta_3 = r/R^{IV} \doteq r/R = \sin\theta$$

$$\beta R \doteq \beta R^{IV}$$

The substitution of these into equations 3.5 - 3.10 after 2.8 and 2.9 have been applied leads to the following far-zone fields for vertical dipoles. These are subject to the same restrictions as 3.5 - 3.10 in addition to $\beta z' << \beta R$.

Case A Hertz dipole above the dielectric at $d \leq z' \leq \infty$, $r' = 0$.

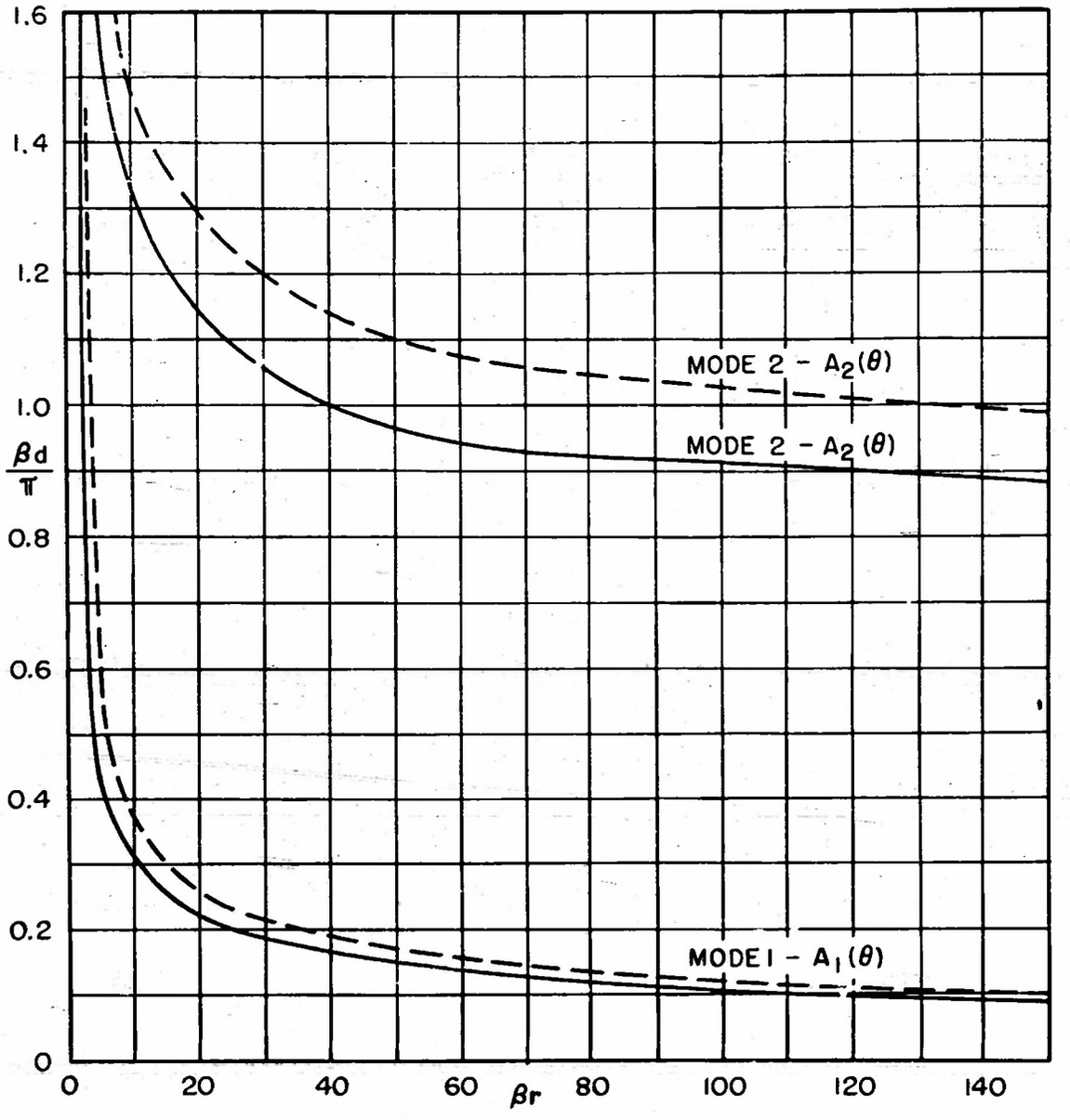

FIG. 5 MINIMUM RADIAL DISTANCE βr AT WHICH THE $A_J(\theta)$ COEFFICIENTS OF THE SURFACE MODES ARE IDENTICALLY 1 FOR ALL Z AS A FUNCTION OF DIELECTRIC THICKNESS βd FOR $0 < \beta d < 1.6\pi$. BASED UPON AN ACCURACY OF 1% OF THE FIELDS AND 0.01% OF THE POYNTING'S VECTOR

$n^2 = 2.54$ ————, $n^2 = 2.25$ — — — —

Region 1.

1. $$\underset{(A)}{\vec{E}_1^{F}}(r,z,z') = \underset{(A)}{\vec{E}_1^{Fr}} + \sum_{J=1}^{k} \underset{(A)}{\vec{E}_{1J}^{FG}}$$

$$= - V [\hat{R} \times \underset{(A)}{B_1^{Fr}}] + \frac{\omega}{\beta^2} \sum_{J=1}^{k} [i\sqrt{\lambda_J^2-\beta^2}\ \underset{(A)}{\vec{B}_{1J}^{FG}} \times \hat{z} - \hat{r} \times \lambda_J \underset{(A)}{\vec{B}_{1J}^{FG}}]$$

2. $$\underset{(A)}{\vec{B}_1^{F}}(r,z,z') = \underset{(A)}{\vec{B}_1^{Fr}} + \sum_{J=1}^{k} \underset{(A)}{\vec{B}_{1J}^{FG}} =$$

$$= - \hat{\Phi}\ \frac{p_1(z')\beta^3 \sin\theta}{2\pi R\omega\varepsilon}\ \frac{[\cos\theta\cos\phi + S\ \sin\phi]}{[\cos\theta - iS\ ]}\ e^{i\beta(R-d\cos\theta]}$$

$$- \frac{\hat{\theta}\ p_1(z')\beta^2}{\omega\varepsilon\sqrt{2\pi r}} \sum_{J=1}^{k} \lambda_J Q(\lambda_J,\beta,n,d)\ e^{[i\lambda_J r-(z+z'-2d)\sqrt{\lambda_J^2-\beta^2}]}$$

Where: $\hat{R}$, $\hat{\theta}$, and $\hat{\Phi}$ are spherical cocrdinates.

$\hat{r}$, $\hat{\theta}$, and $\hat{z}$ are cylindrical coordinates.

$V = (\varepsilon\mu)^{-\frac{1}{2}}$ = the characteristic velocity of medium I.

$\phi = \phi(B,\lambda,z',\theta) = \beta(d-z')\cos\theta$.

$S = S(n,\theta,d,\beta) = n^{-2}\sqrt{n^2-\sin^2\theta}\ \tan(\beta d\sqrt{n^2-\sin^2\theta})$.

Region 2.

3. $$\underset{(A)}{\vec{E}_2^{F}}(r,z,z') = \sum_{J=1}^{k} \underset{(A)}{\vec{E}_{2J}^{FG}}$$

$$= \frac{\omega}{n^2\beta^2} \sum_{J=1}^{k} \left[i\sqrt{n^2\beta^2-\lambda_J^2}\ \tan(z\sqrt{n^2\beta^2-\lambda_J^2})\underset{(A)}{B_{2J}^{FG}} \times \hat{z} - \hat{r} \times \lambda_J \underset{(A)}{B_{2J}^{FG}} \right]$$

4. $$B_{2(A)}^{F}(r,z,z') = \sum_{J=1}^{k} B_{2J}^{FG}(r,z,z')$$

$$= -\frac{\hat{\theta}\, p_1(z')\beta^2}{\omega\varepsilon\sqrt{2\pi r}} \sum_{J=1}^{k} \lambda_J Q(\lambda_J\beta,n,d) e^{[i\lambda_J r-(z'-d)\sqrt{\lambda_J^2-\beta^2}]} \cdot \frac{[\cos(z\sqrt{n^2\beta^2-\lambda_J^2}]}{[\cos(d\sqrt{n^2\beta^2-\lambda_J^2}]}$$

Case B. Hertz dipole in the dielectric at $0 < z' \leq d$, $r' = 0$.

Region 1.

5. $$\vec{E}_{1(B)}^{F}(r,z,z') = \vec{E}_{1(B)}^{Fr}(r,z,z') + \sum_{J=1}^{k} \vec{E}_{1J(B)}^{FG}(r,z,z')$$

$$= -V(\hat{R} \times \vec{B}_{1(B)}^{Fr}) + \frac{\omega}{\beta^2} \sum_{J=1}^{k} [i\sqrt{\lambda_J^2-\beta^2}\ \vec{B}_{1J(B)}^{FG} \times \hat{z} - \hat{r} \times \lambda_J \vec{B}_{1J(B)}^{FG}]$$

6. $$\vec{B}_{1(B)}^{F}(r,z,z') = \vec{B}_{1(E)}^{Fr}(r,z,z') + \sum_{J=1}^{k} \vec{B}_{1J(B)}(r,z,z')$$

$$= -\hat{\Phi}\frac{p_2(z')\beta^3}{2\pi\omega n^2\varepsilon R} \frac{[\sin\theta\cos\theta][\cos(\beta z'\sqrt{n^2-\sin^2\theta})\, e^{i\beta(R-d\cos\theta)}]}{[\cos\theta-iS]\,[\cos(\beta d\sqrt{n^2-\sin^2\theta})\,]}$$

$$-\hat{\theta}\frac{p_2(z')\beta^2}{\omega n^2\varepsilon\sqrt{2\pi r}} \sum_{J=1}^{k} \lambda_J Q(\lambda_J,\beta,n,d)\, e^{[i\lambda_J r-(z-d)\sqrt{\lambda_J^2-\beta^2}]} \cdot \frac{\cos(z'\sqrt{n^2\beta^2-\lambda_J^2})}{\cos(d\sqrt{n^2\beta^2-\lambda_J^2})}$$

Region 2

7. $$\vec{E}_{2(B)}^{F}(r,z,z') = \sum_{J=1}^{k} \vec{E}_{2J(B)}^{F6}(r,z,z')$$

$$= \frac{\omega}{n^2\beta^2} \sum_{J=1}^{k} [i\sqrt{n^2\beta^2-\lambda_J^2}\,\tan(z\sqrt{n^2\beta^2-\lambda_J^2})\,\underset{(B)}{B_{2J}^{FG}} \times \hat{z} - \hat{r} \times \lambda_J \underset{(B)}{B_{2J}^{FG}}]$$

8. $$\underset{(B)}{B_2^F}(r,z,z') = \sum_{J=1}^{k} \underset{(B)}{B_{2J}^{FG}}(r,z,z')$$

$$= -\hat{\theta}\frac{p_2(z')\beta^2}{\omega n^2 \varepsilon \sqrt{2\pi r}} \sum_{J=1}^{k} \lambda_J Q(\lambda_J,\beta,n,d) e^{i\lambda_J r} \cdot$$

$$\frac{\cos(z'\sqrt{n^2\beta^2-\lambda_J^2})\cos(z\sqrt{n^2\beta^2-\lambda_J^2})}{\cos^2(d\sqrt{n^2\beta^2-\lambda_J^2})}$$

Case C. Abraham dipole on the metal at $z' = 0$, $r' = 0$.

The respective quantities are given by the following relations:

9. $$\underset{(C)}{\vec{E}^F}(r,z,0) = \frac{1}{2} \lim_{z' \to 0} \underset{(B)}{\vec{E}^F}(r,z,z')$$

10. $$\underset{(C)}{\vec{B}^F}(r,z,0) = \frac{1}{2} \lim_{z' \to 0} \underset{(B)}{\vec{B}^F}(r,z,z')$$

with subscripts 1 or 2.

It is to be noted that the radiating or compensating terms are waves of spherical type which attenuate as R^{-1}; the guided terms are waves of cylindrical type which attenuate as $r^{-\frac{1}{2}}$. As r or R increases, the ratio of the magnitude of the guided wave to that of the radiated wave increases.

The guided modes are elliptically polarized in region 1 with semi-major axis in the z direction and semi-minor axis along r. The eccentricity for each mode, which is independent of position, is:

11. $$e = \beta/\lambda_J$$

The guided modes are sometimes referred to as "slow waves" because their phase velocities, $V_J = \omega/\lambda_J$, are less than the characteristic velocities of the region 1.

Goubau[16,17] and Attwood[4] have treated, at length, the field and flux distributions for waves of this type.

V

Field Patterns

The field patterns are curves of the relative magnitudes (with respect to their maxima) of the θ-components of the E-fields in region 1, as functions of θ, in the range of θ between 0 and $\pi/2$, for $\beta R >> 1$. The dielectric is assumed to be thin so that $\theta \doteq \pi/2$ along the surface between region 1 and 2, Fig. 2. To obtain the formulas from which these curves are computed, it is necessary to convert the guided components of the fields, equations 4.1 - 4.10 to spherical coordinates and to recombine the fields at some large fixed βR.

It is important to notice that the field patterns defined above are those measured by a receiving antenna polarized and traveling in the θ-direction at the chosen βR. Since the guided waves have R components, the patterns are not the relative magnitudes of the total field along the great circle of radius βR. It is also important to observe the manner in which these patterns vary with βR. Since the radiated wave disappears at $\theta \doteq \pi/2$, while for most finite dielectric thicknesses, βd, the surface wave attenuates rapidly with decreasing θ, the region of interference between the two is very small. For these reasons, the principal effect of varying βR, is to vary the relative magnitudes of the sections of the field patterns, at θ near $\pi/2$ and at θ less than $\pi/2$, by a factor $R^{\frac{1}{2}}$.

Figures 6 - 14 contain field patterns for cases A, B, and C, $n^2 = 2.54$, $\beta R \doteq 239$ and various βd and $\beta z'$, on semi-logarithmic scales, with comparison patterns for dipoles above

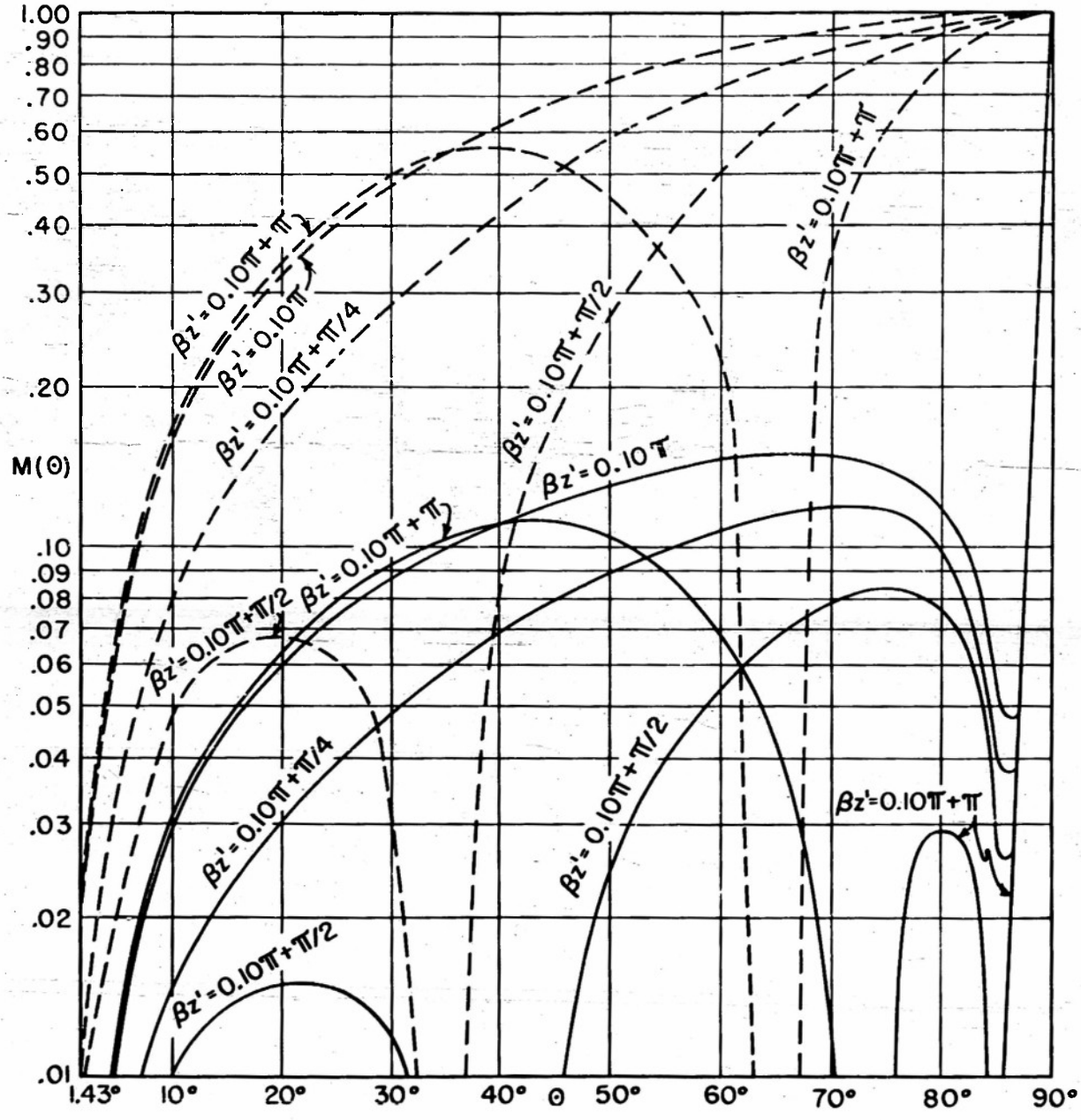

FIG. 6 FIELD PATTERNS FOR CASE A, $\beta d = 0.10\pi$, M(θ) VS. θ WITH FIELD PATTERNS WITH $\beta d = 0$ FOR COMPARISON. $\beta R_0 \doteq 239$, $n^2 = 2.54$, $\beta d = 0.10\pi$ ———, $\beta d = 0$ – – – –
$\beta z' = 0.10\pi$, $\pi/4 + 0.10\pi$, $\pi/2 + 0.10\pi$, $\pi + 0.10\pi$

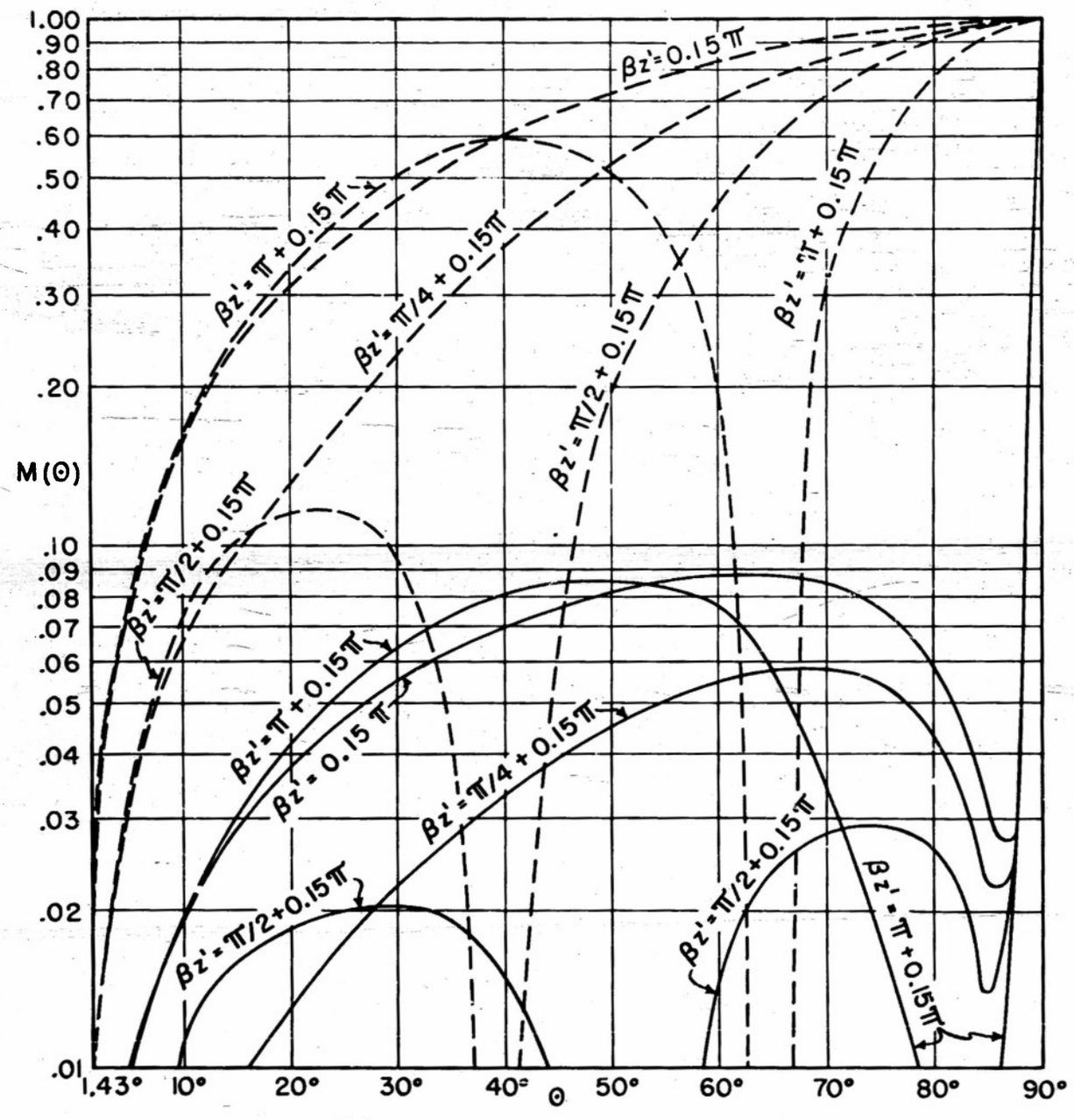

FIG. 7 FIELD PATTERNS FOR CASE A, $\beta d = 0.15\pi$, M(Θ) VS. Θ WITH FIELD PATTERNS WITH $\beta d = 0$ FOR COMPARISON
$\beta R_0 \doteq 239$, $n^2 = 2.54$, $\beta d = 0.15\pi$ ——, $\beta d = 0$ – – – –
$\beta z' = 0.15\pi, \pi/4 + 0.15\pi, \pi/2 + 0.15\pi, \pi + 0.15\pi$

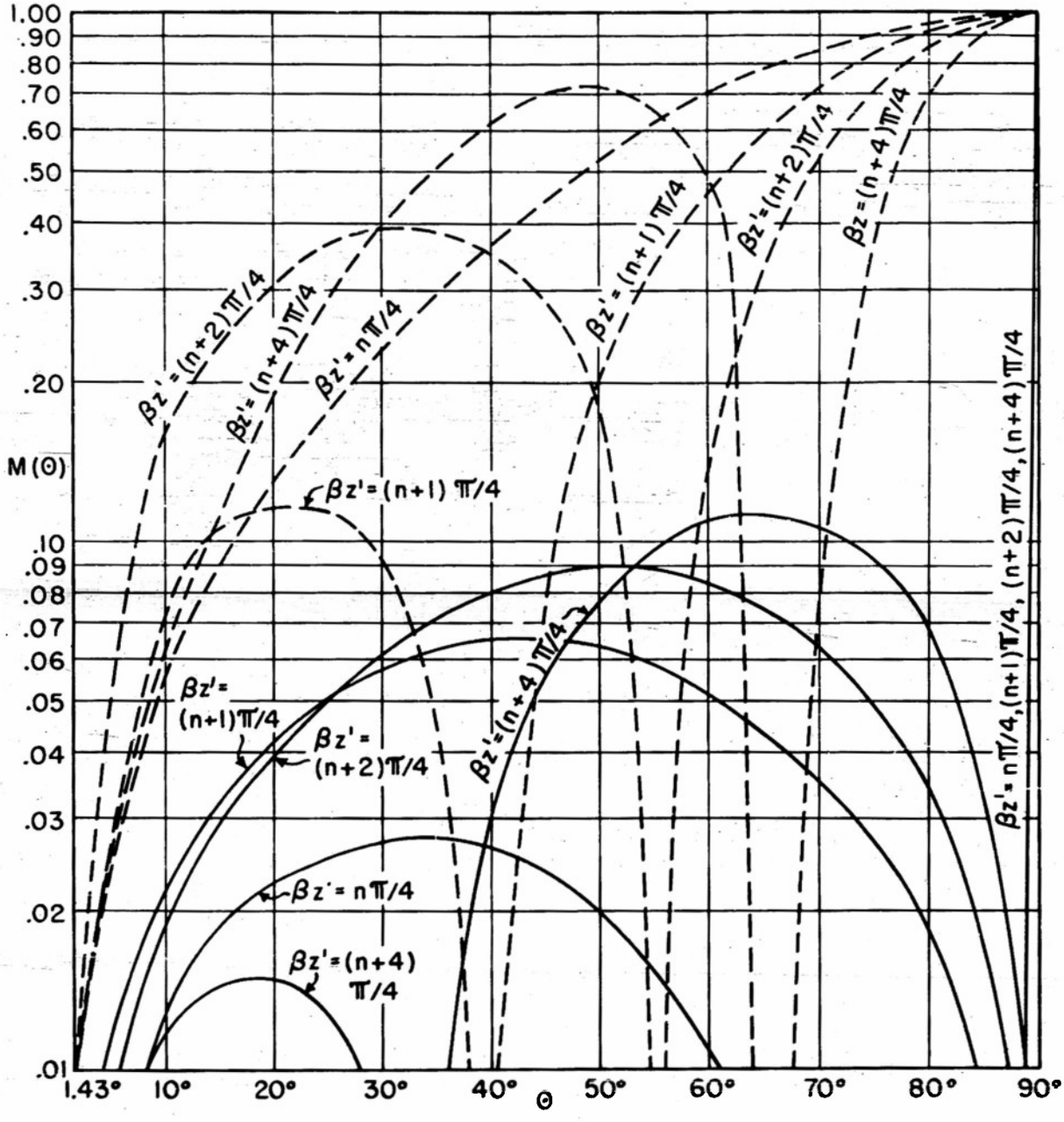

FIG. 8 FIELD PATTERNS FOR CASE A, $\beta d = n\pi/4$, M(0) VS. 0, WITH FIELD PATTERNS WITH $\beta d = 0$ FOR COMPARISON

$\beta R_0 \doteq 239$, $n^2 = 2.54$, $\beta d = n\pi/4$ ———— , $\beta d = 0$ – – – –

$\beta z' = n\pi/4, (n+1)\pi/4, (n+2)\pi/4, (n+4)\pi/4$

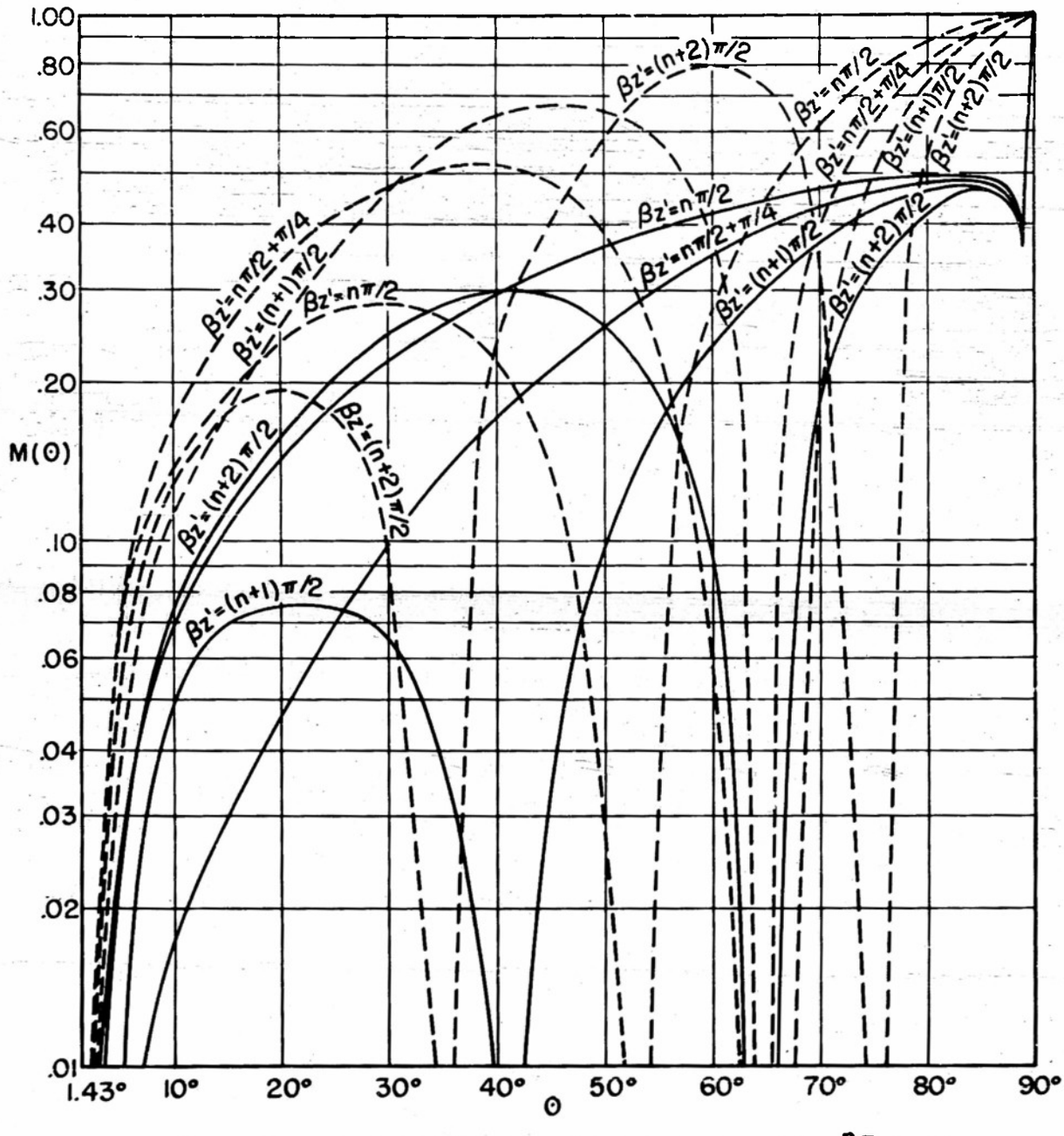

FIG. 9 FIELD PATTERNS FOR CASE A, $\beta d = \frac{n\pi}{2}$ WITH FIELD PATTERNS WITH $\beta d = 0$ FOR COMPARISON $\beta R_0 = 239$, $n^2 = 254$, $\beta d = \frac{n\pi}{2}$ —, $\beta d = 0$ ---, $\beta z' = \frac{n\pi}{2}, \frac{n\pi}{2} + \frac{\pi}{4}, (n+1)\frac{\pi}{2}, (n+2)\frac{\pi}{2}$

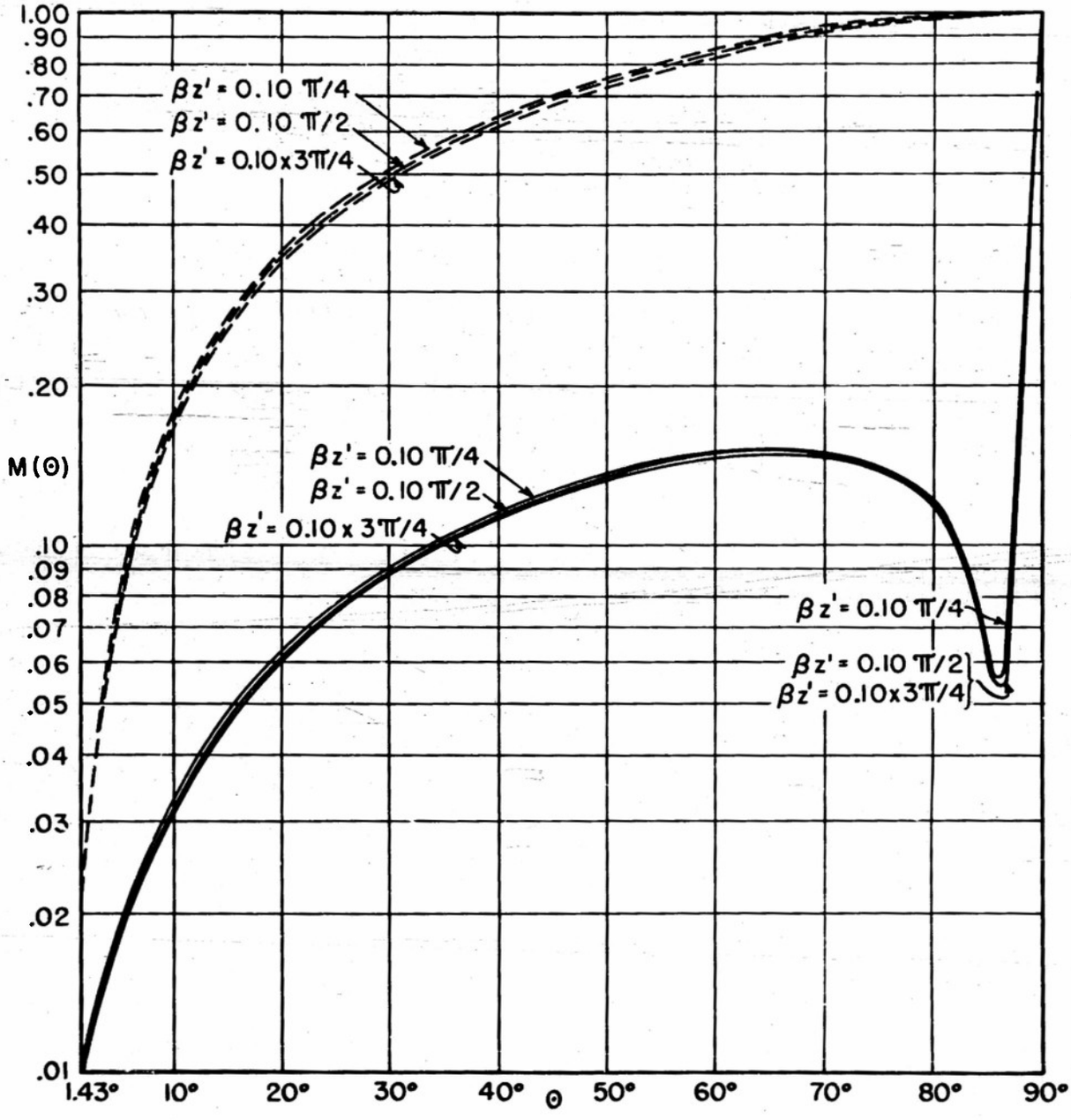

FIG. 10 FIELD PATTERNS FOR CASE B, $\beta d = 0.10\pi$, $n(\Theta)$ VS. Θ WITH FIELD PATTERNS WITH $\beta d = 0$ FOR COMPARISON. $\beta R_0 \doteq 239$, $n^2 = 2.54$, $\beta d = 0.10\pi$ ———, $\beta d = 0$ – – – – $\beta z' = 0.10\pi/4$, $0.10\pi/2$, $0.10 \times 3\pi/4$

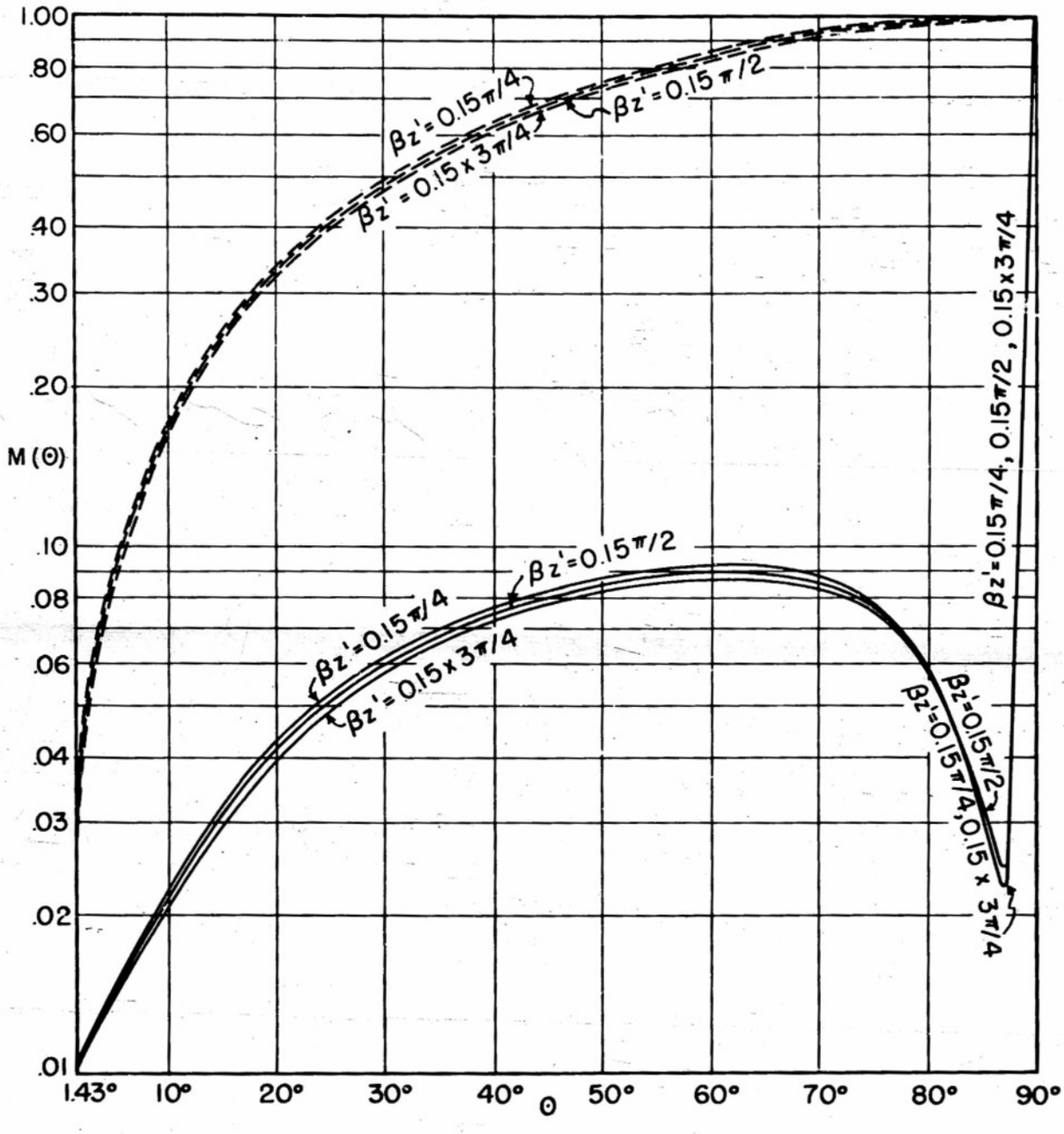

FIG. 11 FIELD PATTERNS FOR CASE B, $\beta d = 0.15\pi$, M(θ) VS θ
WITH FIELD PATTERNS WITH $\beta d = 0$ FOR COMPARISON
$\beta R \doteq 239$, $n = 2.54$, $\beta d = 0.15\pi$ —, $\beta d = 0$ ---
$\beta z' = 0.15\frac{\pi}{4}$, $0.15\frac{\pi}{2}$, $0.15 \times \frac{3\pi}{4}$

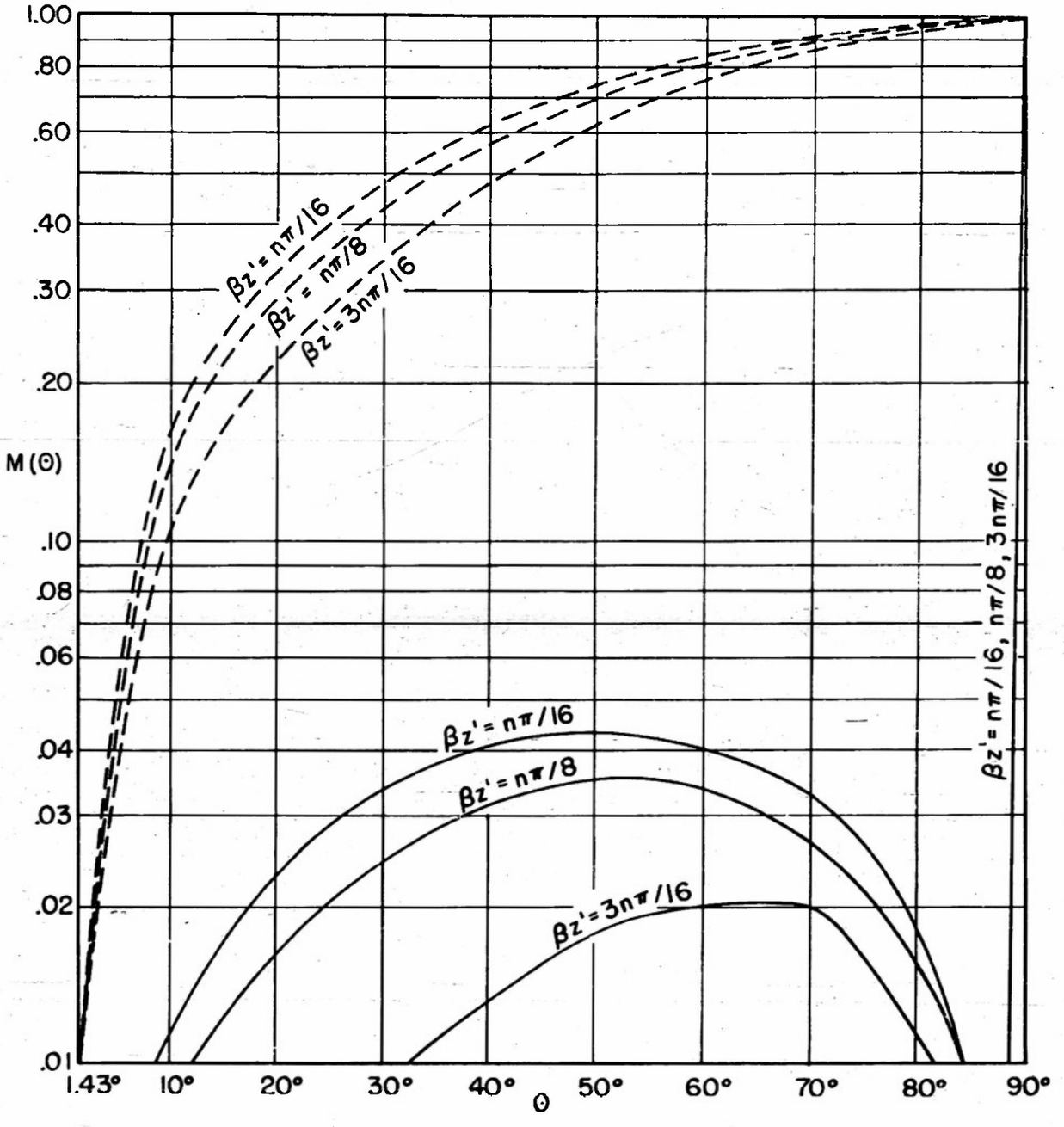

FIG. 12 FIELD PATTERNS FOR CASE B, $\beta d = \frac{n\pi}{4}$, M(θ) VS. θ WITH FIELD PATTERNS WITH $\beta d = 0$ FOR COMPARISON $\beta R_0 \doteq 239$, $n^2 = 2.54$, $\beta d = \frac{n\pi}{4}$ —, $\beta d = 0$ ---, $\beta z' = \frac{n\pi}{16}, \frac{n\pi}{8}, \frac{3n\pi}{16}$

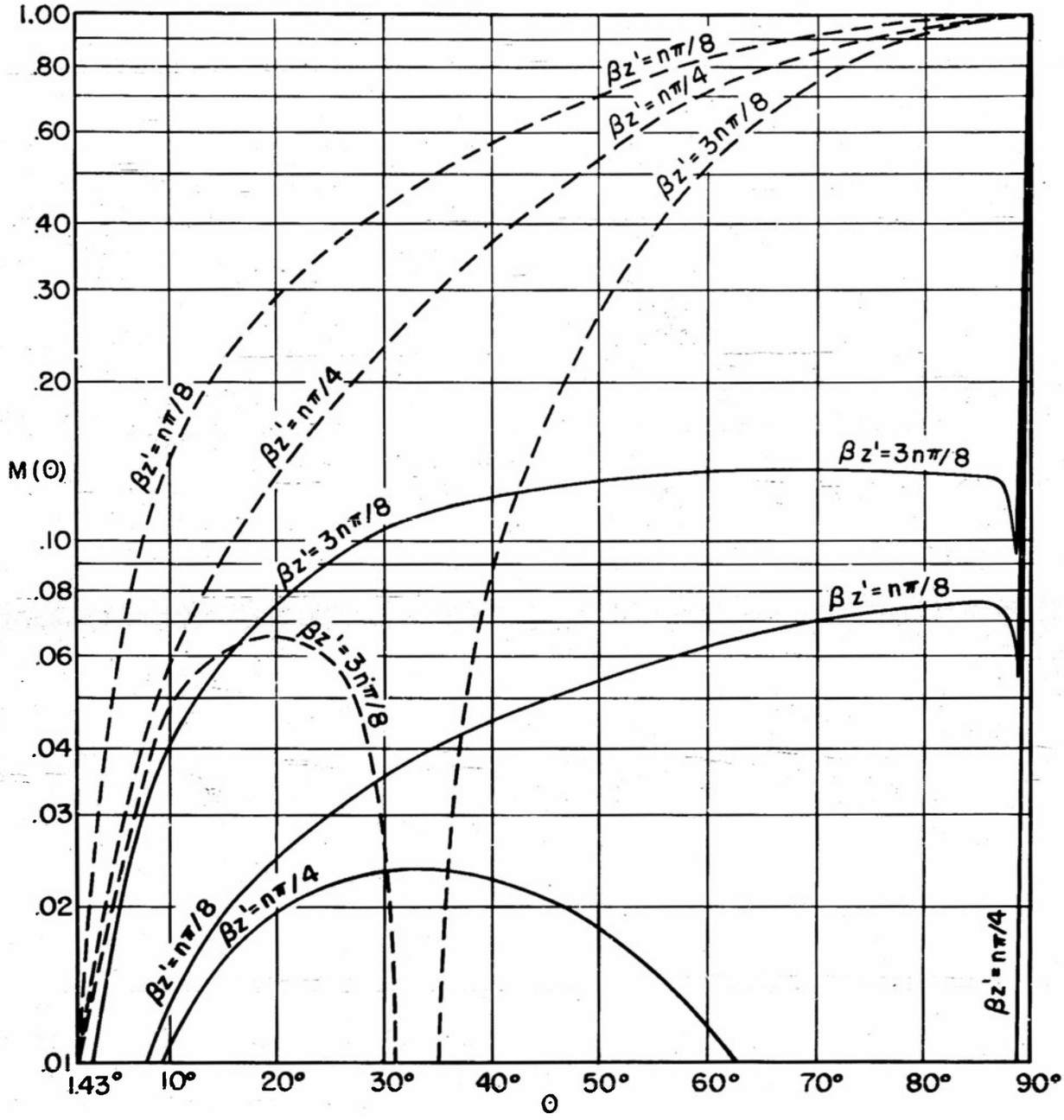

FIG. 13 FIELD PATTERNS FOR CASE B, $\beta d = \frac{n\pi}{2}$, M(0) VS. θ WITH FIELD PATTERNS WITH $\beta d = 0$ FOR COMPARISON $\beta R_0 = 239$, $n^2 = 2.54$, $\beta d = \frac{n\pi}{2}$ —, $\beta d = 0$ ---
$\beta z' = \frac{n\pi}{4}, \frac{n\pi}{8}, \frac{3n\pi}{4}$

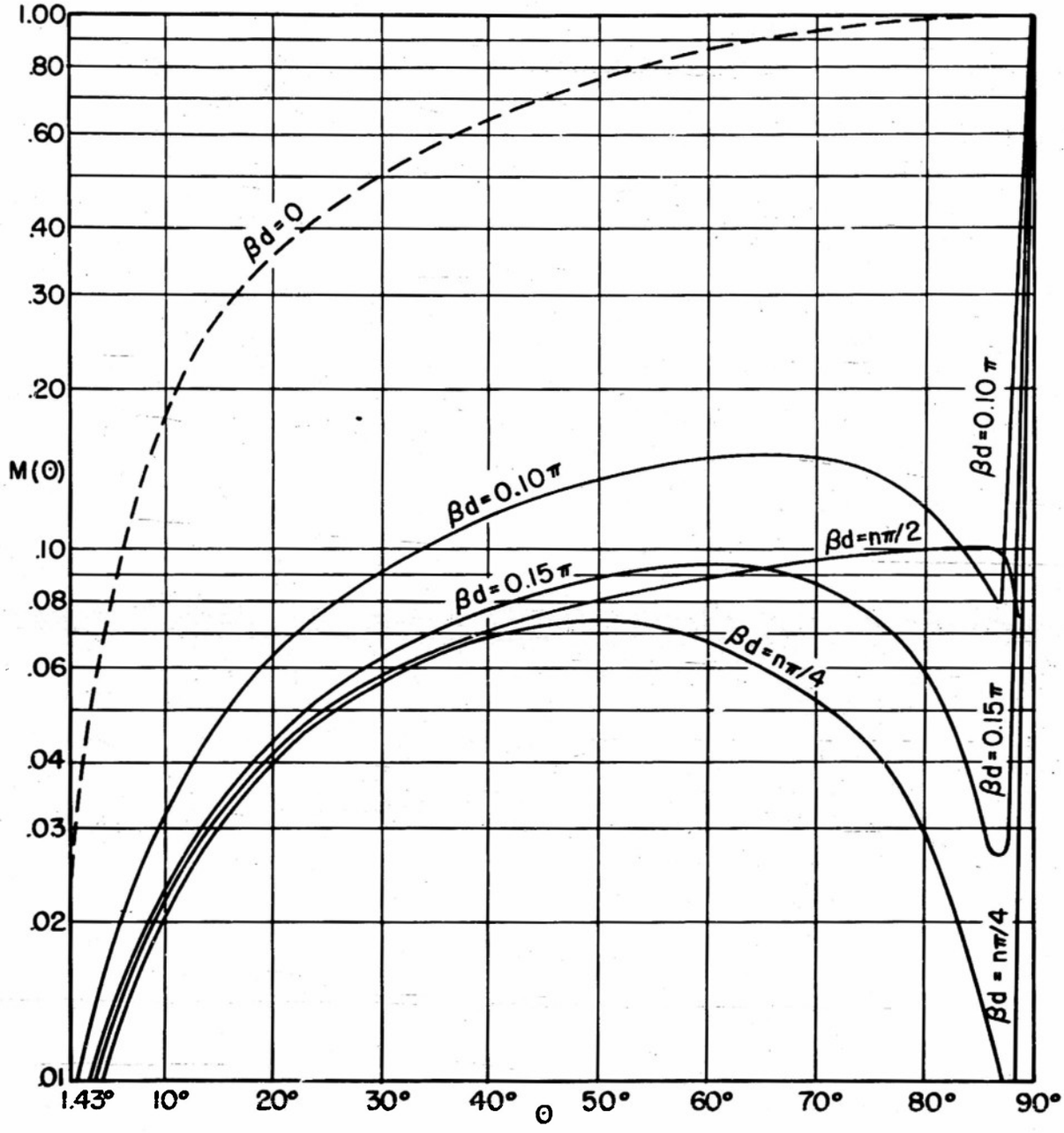

FIG. 14 FIELD PATTERNS FOR CASE C, $\beta z' = 0$, M(0) VS. θ
WITH FIELD PATTERN WITH $\beta d = 0$ FOR COMPARISON
$\beta R = 239, n = 2.54, \beta d = 0$ ---, $\beta d = 0.10\pi, 0.15\pi, \frac{n\pi}{4}, \frac{n\pi}{2}$ —

or on a perfect, uncoated conductor for the same dipole heights, $\beta z'$, as those with the coating present.

The dielectric constant of polystyrene was chosen as being typical. $\beta R \doteq 239$ was not only chosen as being typical but was chosen for proposed future experimental use. The thickness $\beta d = n\pi/2$ may seem peculiar, but in Fig. 4 this value is seen to be smaller than, but very close to, $\pi/\sqrt{n^2-1}$, the value at which multimode propagation commences. Since the value $\beta d = n\pi/2$ possesses this quality, besides being convenient for numerical computation, it was chosen. It is clear that the dielectric thicknesses used provide good coverage of the region of single-mode propagation.

The quantities plotted in Figs. 6 - 14 are:

1. $$M(\theta) = \frac{\left|E_{\theta_1}^{F}\right|}{\left|E_{\theta_1}\right| \theta = \pi/2 = \theta_{max}}$$

For $\beta d = 0$ and $\beta d \neq 0$.

The main points of interest in Figs. 6 - 14 are the large maxima or spikes at $\theta = \pi/2$ and the compressions of the rest of the fields with the accompanying minima between these two. These curves are drawn on a logarithmic scale and must be examined closely to appreciate the actual large magnitudes of the maxima at $\theta = \pi/2$ (the surface waves) compared to the rest of the patterns (the radiated waves). The ratios of the powers in the two components of the fields, Figs. 20 and 21, give a better conception of the large size of these maxima, especially if consideration is given to the fact that the surface wave is compressed into a small segment of space, while the radiated wave is dispersed over the complete half-space.

For case A the field patterns for $\theta < \pi/2$ are similar to those without the dielectric coating for dipole heights equal to the dipole heights in case A minus the dielectric thickness.

This means that, for case A, the radiated waves are strongly reflected by the dielectric surface.

In cases B and C the effect of the dielectric is to compress the radiated wave into a smaller sector.

Figure 15 is a plot of $\left|E_{\theta}^{FG}\right| / \left|E_{RJ}^{FG}\right|$ versus θ for the βd's of Figs. 6 - 14 over the range of significant magnitudes of E_J^{FG}. For the cases considered $J = 1$. These yield an indication of the magnitudes of the R-components of the radiation patterns. For the thicker dielectrics these ratios are almost constant, indicating that, since $\left|E_{zJ}\right| / \left|E_{zJ}^{FG}\right|$ is constant and equal to the θ to R component ratios of Fig. 15 at $\theta = \pi/2$, $E_{\theta J}^{FG}$ and E_{RJ}^{FG} are essentially E_{zJ}^{FG} and E_{rJ}^{FG} respectively over the range of significant values of $\left|E_J^{FG}\right|$.

VI

Formulation of the Power Equation

The purpose of this section is to formulate the equations which govern the time-average flow of power across a surface surrounding the source $p(z')$. Since the far-zone approximations do not satisfy Maxwell's equations and since the proofs that the powers in the guided-and radiated-type waves are independent require the fields to satisfy Maxwell's equations, it is necessary to formulate the exact fields.

Consider $\vec{E}$ and $\vec{B}$, the exact fields existing in the configuration of Fig. 1, due to a source $p(z')$ in any of three positions A, B, or C of Fig. 1.

For $\beta r > 0$ the transformation of equations 2.29 - 2.34 to the Hankel function form 3.1, is valid. The exact integrations, if they could be performed, would be taken over paths W_1 and W_2 of Fig. 3. These integrations yield contributions from the poles and branch cuts. The application of equations 2.8 and 2.9 to the results of the integrations yields the exact E-and B-fields. It is sufficient for the purposes of this section to represent the branch-cut contributions. $\vec{E}^r$, $\vec{B}^r$, symbolically, while the contributions of the poles, $\vec{E}^G$, $\vec{B}^G$, may be explicitly evaluated.

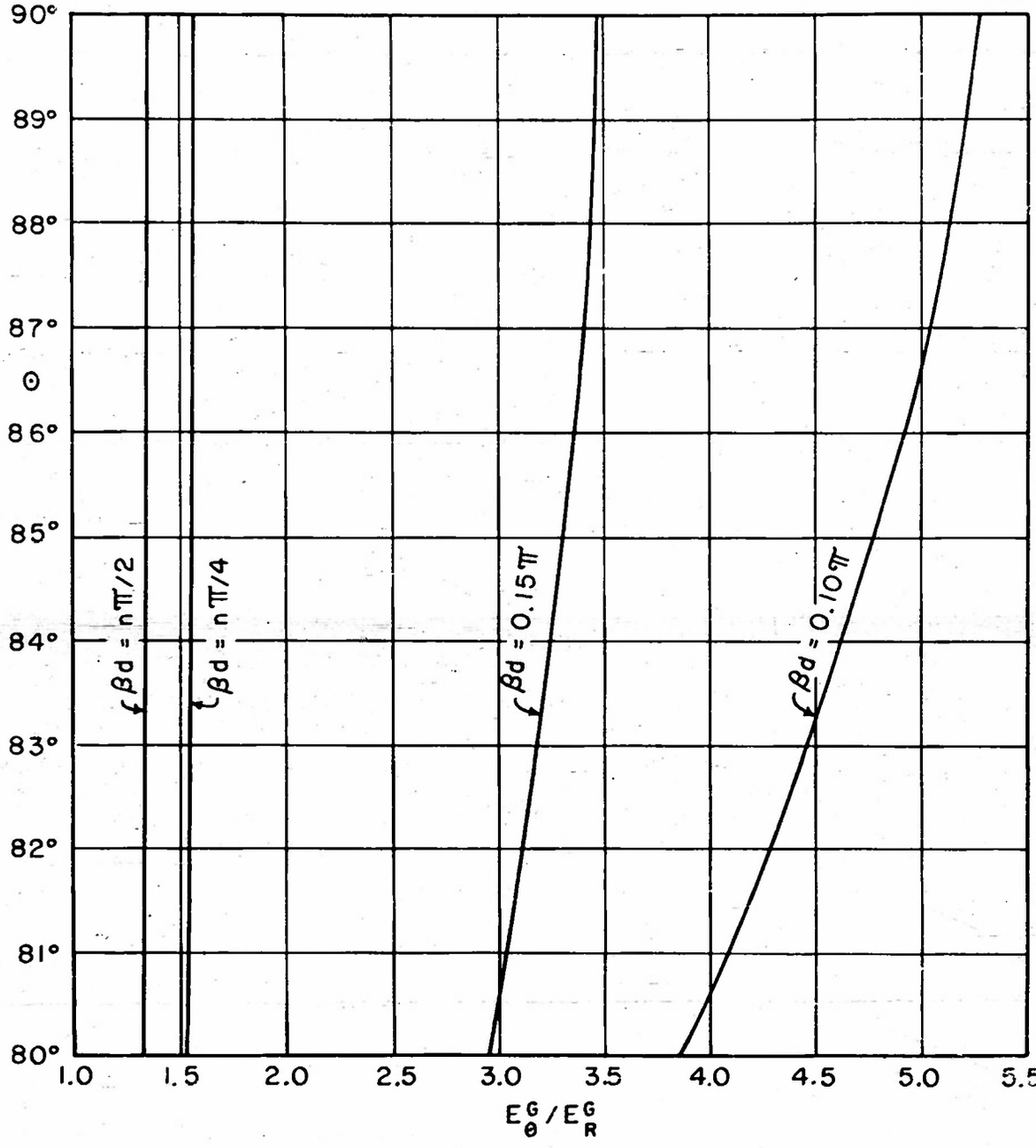

FIG. 15 E_θ^G / E_R^G VS. θ OVER THE RANGE OF SIGNIFICANT VALUES OF $|E^G|$ FOR $\beta d = n\pi/2, n\pi/4, 0.15\pi, 0.10\pi$ AND FOR $n^2 = 2.54$

For $\beta r > 0$ the exact fields may be represented by:

1. a) $\vec{E} = \vec{E}^r + \vec{E}^G$ b) $\vec{B} = \vec{B}^r + \vec{B}^G$

2.

a) $$\vec{E}^G = \sum_{J=1}^{k} \vec{E}_J^G$$

$$= \sum_{J=1}^{k} \begin{cases} A_{1J}\, e^{in/2}[\hat{r}\sqrt{\lambda_J^2-\beta^2}\, H_1^1(\lambda_J r) + \hat{z}\lambda_J H_o^1(\lambda_J r)]e^{-z\sqrt{\lambda_J^2-\beta^2}} & \text{Region 1} \\ A_{2J}\, e^{in/2}[\hat{r}\sqrt{n^2\beta^2-\lambda_J^2}\, \sin(z\sqrt{n^2\beta^2-\lambda_J^2}\, H_1^1(\lambda_J r) \\ \quad + \hat{z}\lambda_J \cos(z\sqrt{n^2\beta^2-\lambda_J^2})\, H_o^1(\lambda_J r)] & \text{Region 2} \end{cases}$$

b) $$\vec{B}^G = \sum_{J=1}^{k} \vec{B}_J^G$$

$$= \sum_{J=1}^{k} \hat{\theta} H_1^1(\lambda_J r)\, \frac{\beta^2}{\omega} \begin{cases} A_{1J}\, e^{-z\sqrt{\lambda_J^2-\beta^2}} & \text{Region 1} \\ A_{2J}\, n^2 \cos(z\sqrt{n^2\beta^2-\lambda_J^2}) & \text{Region 2} \end{cases}$$

Where A_J is a function of λ_J, B, n, d, ω, z' and p(z').

For $\beta R >> 1$

3. a) $$\lim_{\beta R >> 1} \begin{Bmatrix} \vec{E} \\ \vec{B} \end{Bmatrix} \doteq \begin{Bmatrix} \vec{E}^F \\ \vec{B}^F \end{Bmatrix}$$

b) $$\lim_{\beta R >> 1} \begin{Bmatrix} \vec{E}^r \\ \vec{B}^r \end{Bmatrix} \doteq \begin{Bmatrix} \vec{E}^{Fr} \\ \vec{B}^{Fr} \end{Bmatrix}$$

c) $$\lim_{\beta R >> 1} \begin{Bmatrix} \vec{E}_J^G \\ \vec{B}_J^G \end{Bmatrix} \doteq \begin{Bmatrix} \vec{E}_J^{FG} \\ \vec{B}_J^{FG} \end{Bmatrix}$$

Where the fields on the right sides are given in section 4. $\vec{E}^F$ and $\vec{B}^F$ are approximate solutions to Maxwell's equations for large βr while $\vec{E}$, $\vec{B}$, $\vec{E}^r$, $\vec{B}^r$, $\vec{E}_J^G$, B_J^G are exact solutions to Maxwell's equations for $\beta R > 0$.

For $\beta r >> 1$ the guided or residue waves exist uncancelled, but as $\beta r \to 0$ the functional forms of the guided waves become infinite. Since this is physically impossible except at discrete points at $r = o$, $z = z'$, the so-called radiating or compensating fields, due to the branch cut contributions, must cancel the singular parts of the guided waves as $\beta r \to 0$. An indication of the cancellation is given by the appearance of the factor $A_J(\theta)$ in the asymptotic results. Despite this cancellation the division in equation 1 is valid because of the linearity of Maxwell's equations.

Since $p(z')$ is arbitrary, let it be chosen to be a real quantity. It may be verified that for $p(z')$ real A_{1J} and A_{2J} are real.

The power flowing across any surface S surrounding the source is given by:

4. $$P = \frac{Re}{2\mu}\left[\int_S \hat{n} \cdot (\vec{E}^r \times \vec{B}^{r*})dS + \sum_{J=1}^{k} \int_S \hat{n} \cdot (\vec{E}^r \times \vec{B}_J^{G*} + \vec{E}_J^G \times \vec{B}^{r*})dS + \sum_{J=1}^{k}\sum_{m=1}^{k} \int_S \hat{n} \cdot (\vec{E}_J^G \times \vec{B}_m^{G*})dS\right]$$

where $\hat{n}$ is the outward normal to the volume enclosed by S, and superscript* indicates the complex conjugate.

It will be proved that

5. $$\frac{Re}{2\mu}\left[\int_S \hat{n} \cdot (\vec{E}^r \times \vec{B}_J^{G*} + \vec{E}_J^G \times \vec{B}^{r*})ds\right] = 0$$

and

6. $$\frac{Re}{2\mu}\int_S \hat{n}\cdot(\vec{E}_J^{\,G}\times\vec{B}_m^{\,G*})dS = 0 \quad J \neq m$$

(The author is indebted to Dr. George Goubau for suggesting these proofs and recommending references to similar proofs.[18, 19]).

Some necessary formulas derived by well-known methods[20] are

7. $$\frac{Re}{2\mu}\int_S \hat{n}\cdot(\vec{E}_A\times\vec{B}_B^{*})dS = \frac{Im\omega}{2}\int_V \vec{P}_B^{\,*}\cdot\vec{E}_A\,dV$$
$$= -\frac{Re}{2}\int_V \vec{J}_B^{\,*}\cdot\vec{E}_A\,dV$$

where S is a closed surface surrounding a volume V.
$\vec{E}_A$, $\vec{B}_A$ and $\vec{E}_B$, $\vec{B}_B$ are two independent solutions to Maxwell's equation in V.
P and J are the impressed polarization and current densities.
ϵ and μ are assumed to be real in V.
n is the outward normal to V.
and the reciprocity condition.[21]

8. $$\int_S \hat{n}\cdot[\vec{E}_A\times\vec{B}_B - \vec{E}_B\times\vec{B}_A]\,dS =$$
$$-i\omega\mu\int_V(\vec{P}_A\cdot\vec{E}_B - \vec{P}_B\cdot\vec{E}_A)dV$$
$$= -\mu\int_V \vec{J}_B\cdot\vec{E}_A - \vec{J}_A\cdot\vec{E}_B)dV$$

Equation 6 will be proved first:

To this end consider the configuration of Fig. 16 agreeing with Fig. 1.

Since the cylinders S_1 and S_2 are semi-infinite and the surface $z = 0$ is a perfect conductor, S may be set equal to S_1 or S_2 in equation (4). It is therefore sufficient to prove

equation (6) over S_1 or S_2.

If $\vec{E}_A = \vec{E}_J^G$ and $\vec{B}_B = \vec{B}_m^G$ are substituted in equation (7) with the volume V_1 as the enclosed volume and noting that the volume V_1, Fig. 16, is sourceless, the following identity is arrived at.

9. $$\frac{Re}{2\mu} \int_{S_1} \hat{r} \cdot (\vec{E}_J^G \times \vec{B}_m^{G*}) dS_1 =$$

$$\frac{Re}{2\mu} \int_{S_2} \hat{r} \cdot (\vec{E}_J^G \times \vec{B}_m^{G*}) dS_2 = \text{constant in } r = K.$$

This is a constant since r_1 and r_2 may be independently varied while the other is fixed or explicitly

10. $$\frac{Re}{2\mu} \int_{S_1 \text{ or } S_2} \hat{r} \cdot (\vec{E}_J^G \times \vec{B}_m^{Gx}) dS_{1 \text{ or } 2} =$$

$$- Re \frac{\pi}{\mu} [i\, r_{1 \text{ or } 2} \lambda_J H_o^1(\lambda_J r_{1 \text{ or } 2}) H_1^2(\lambda_m r_{1 \text{ or } 2})] D_{Jm} = K$$

where the constant D_Jm is:

$$D_{Jm} = \frac{\beta^2}{\omega} \left\{ \int_d^\infty A_{1J} A_{1m} \exp[-z(\sqrt{\lambda_J^2-\beta^2} + \sqrt{\lambda_m^2-\beta^2})] dz \right.$$

$$\left. + \int_0^d n^2 A_{2J} A_{2m} \cos(z\sqrt{n^2\beta^2-\lambda_J^2}) \cos(z\sqrt{n^2\beta^2-\lambda_m^2}) dz \right\}$$

Specifically, this is true for large βr where the asymptotic forms of the Hankel functions are valid:

11. $$\lim_{\beta r \gg 1} K = D_{Jm} \sqrt{\frac{\lambda_J}{\lambda_m}} \cos(r(\lambda_J - \lambda_m))$$

For $\lambda_J \neq \lambda_m$, this is zero for $r = \frac{q\pi}{2(\lambda_J - \lambda_m)}$,

where q = integers, but K is a constant; hence the constant must be zero. Thus equation (6) is verified, since D_{Jm}, $J \neq m$,

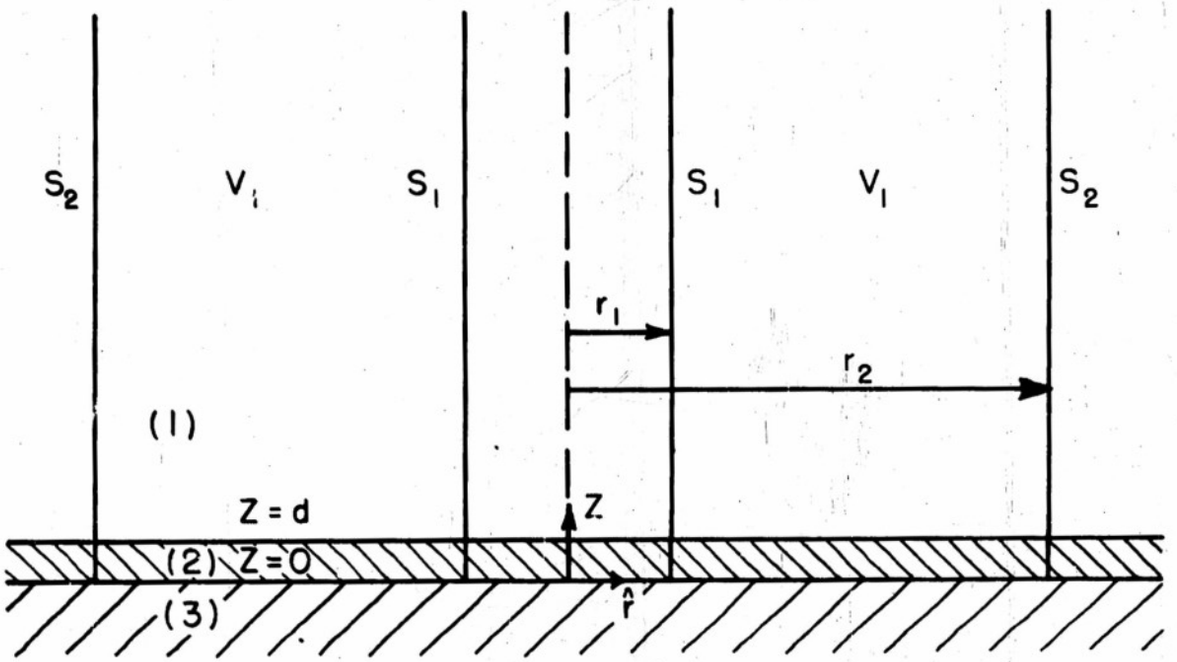

FIG. 16 CONCENTRIC CYLINDRICAL SURFACES OF INFINITE HEIGHT S_1 AND S_2

must be zero for K to be zero for all $r > o$.

Equation (5) will now be proved:

Consider the configuration of Fig. 17. The source $p(z')$ may be in region 1 or 2 or half-submerged in the conductor at $z = o$, i.e., an Abraham dipole. The current $I(z")$ on the semi-infinite cylinder V_2 is such as to excite only the Jth guided mode.

After utilizing the representations of the Hankel functions for small arguments the following representation for $I(z")$ is arrived at.

$$12. \quad I_z(z") = -\frac{i4\beta^2}{\omega\lambda_J\mu} \begin{cases} A_{1J}\, e^{-z"\sqrt{\lambda_J^2-\beta^2}} & d \leq z" < \infty. \\ A_{2J}\, n^2 \cos(z"\sqrt{n^2\beta^2-\lambda_J^2}) & \theta \leq z" \leq d. \end{cases}$$

This current excites only $\vec{E}_J^G(r_1,z)$ and $\vec{B}_J^G(r_1z)$. The dipole excites $\vec{E}(r_o,z)$ and $\vec{B}(r_o,z)$.

The subscripts for cases A, B, or C agree throughout. It is assumed that $I_z(z")$ is the total current on F_2 and $p(z')$ is the total polarization in V_1.

The application of equation (8) to V_1, F_1, noting that the polarization, $\vec{P}$, is a constant times a delta-function, leads to

$$13. \quad \int_{F_1} \hat{n} \cdot [\vec{E} \times \vec{B}_J^G - \vec{E}_J^G \times \vec{B}]dF_1 =$$

$$\omega\mu\, \lambda_J H_o^1(\lambda_J x) \begin{cases} p_1(z')A_{1J}\, e^{-z'\sqrt{\lambda_J^2-\beta^2}} & d \leq z' \leq \infty \\ p_2(z')A_{2J}\cos(z'\sqrt{n^2\beta^2-\lambda_J^2}) & 0 \leq z' \leq d \\ \frac{p_2(0)A_{2J}}{2} & z' = 0 \end{cases}$$

The application of equation (8) to V_2, F_2 in the light of the orthogonality condition, equation 6, gives

14. $$\int_{F_2} n \cdot [\vec{E} \times \vec{B}_J^G - \vec{E}_J^G \times \vec{B}]\, dF_2 =$$

$$= \mu \int_0^\infty I(z'')E_z^r(x,z'')dz''$$

$$- \frac{2\beta^2}{\omega} H_o^1(\lambda_J x) \left\{ n^2 A_{2J}^2\, d + n^2 \frac{A_{2J}^2 \sin(2d\sqrt{n^2\beta^2 - \lambda_J^2})}{2\sqrt{n^2\beta^2 - \lambda_J^2}} \right.$$

$$\left. + \frac{A_{1J}^2\, e^{-2d\sqrt{\lambda_J^2 - \beta^2}}}{\sqrt{\lambda_J^2 - \beta^2}} \right\}$$

The application of equation (8) to the sourceless region V_3, noting that the integrations over the surfaces at infinity and at $z = 0$ vanish, and rearranging the resulting equation leads to:

15. $$\frac{\mu \int_0^\infty I(z'')E_z^r dz''}{H_o^1(\lambda_J x)} =$$

$$- \frac{2\beta^2}{\omega} \left[n^2 A_{2J}^2 d + n^2 \frac{A_{2J}^2 \sin(2d\sqrt{n^2\beta^2 - \lambda_J^2})}{2\sqrt{n^2\beta^2 - \lambda_J^2}} + \frac{A_{1J}^2\, e^{-2d\sqrt{\lambda_J^2 - \beta^2}}}{\sqrt{\lambda_J^2 - \beta^2}} \right.$$

$$+ \omega\mu\lambda_J \begin{cases} p_1(z')\, A_{1J}\, e^{-z'\sqrt{\lambda_J^2 - \beta^2}} & d \le z' \le \infty \\ p_2(z')\, A_{2J} \cos(z'\sqrt{n^2\beta^2 - \lambda_J^2}) & 0 \le z' \le d \\ \frac{P_2(0)A_{2J}}{2} & z' = 0 \end{cases}$$

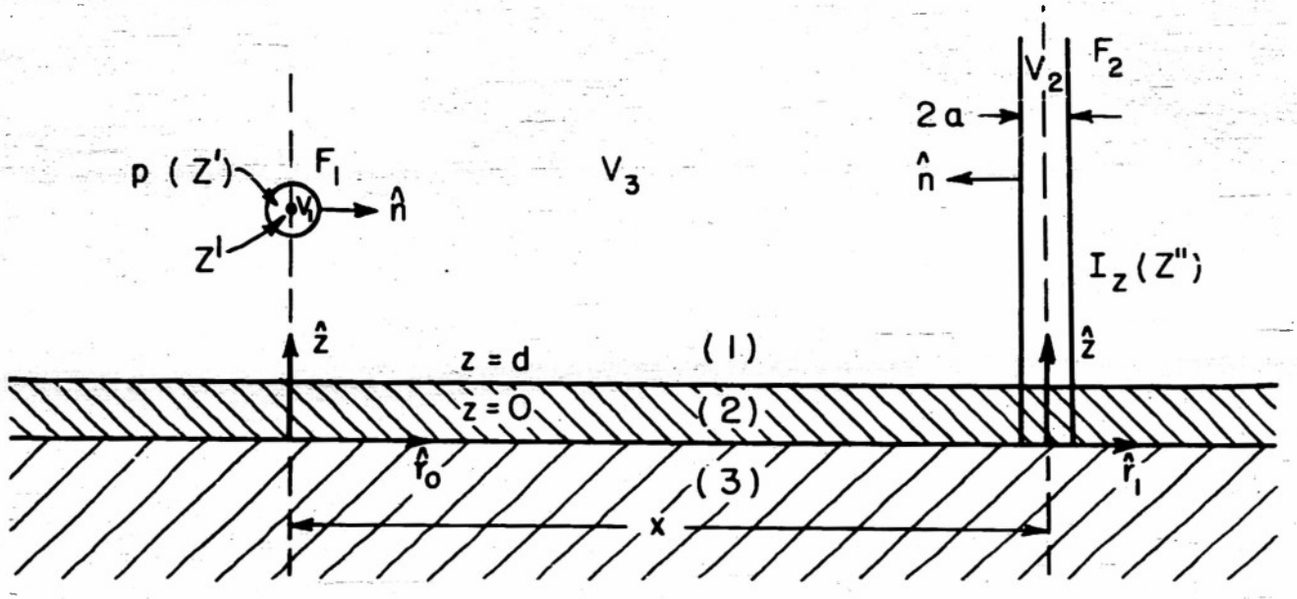

FIG. 17 NARROW CYLINDER OF INFINITE HEIGHT SUPPORTING CURRENT $I_z(Z'')$ AND SPHERICAL SURFACE SURROUNDING $p(Z')$ SEPARATED BY DISTANCE x

The right side of equation (15) is not a function x or z. Hence, the equation is equal to a constant, G, in x and z.

As βx becomes large, $\beta x >> 1$; the quantities on the left side of equation (15) approach zero in the following manner:

$$\beta x \overset{\lim}{>>} 1 \quad E_z^r(x,z'') \sim \frac{1}{\sqrt{x^2+z''^2}}$$

$$\beta x \overset{\lim}{>>} 1 \quad H_o^1(\lambda_J x) \sim \frac{1}{\sqrt{x}}$$

Hence:

16. $$\lim_{\beta x \to \infty} \frac{G}{\mu} = \lim_{\beta x \to \infty} \frac{\int_0^\infty I(z'')E_z^r dz''}{H_o^1(\lambda_J x)} = 0.$$

Since G is a constant, then $G \equiv 0$ and both sides of (15) are identically zero.

It is enlightening to observe that the right side of (15) when set equal to zero offers an alternate method of determining the A_J's. The author has verified the fact that the A_J's are identical when derived by both methods. This offers a check on the paths of integration chosen in Fig. 3.

Since the denominator of the right side of equation (16) is well behaved, $\lambda_J x > 0$, the numerator is zero.

With the substitution of the right side of (12) for I(z'') the numerator on the right side of equation 16 becomes:

17. $$A_{2J}\, n^2 \int_0^d E_z^r(x,z'')\cos(z''\sqrt{n^2\beta^2-\lambda_J^2})dz''$$

$$+ A_{1J} \int_d^\infty E_z^r(x,z'')e^{-z''\sqrt{\lambda_J^2-\beta^2}}\, dz'' = 0.$$

The following integral is to be considered with reference to Fig. 16.

18. $$\frac{Re}{2\mu} \int_{\substack{S_1 \\ \text{or} \\ 2}} \hat{n} \cdot [\vec{E}^r(r,z,z') \times \vec{B}_J^{G*}(r,z,z')]d S_{\substack{1 \\ \text{or} \\ 2}}$$

$$= - \frac{Re\pi}{\mu} \left\{ r_{\substack{1 \\ \text{or} \\ 2}} \frac{\beta^2}{\omega} H_1^1(\lambda_J r_{\substack{1 \\ \text{or} \\ 2}}) \right\} \left\{ A_{1J} \int_d^\infty E_z^r \Big|_{r = r_1 \text{ or } r_2} e^{-z\sqrt{\lambda_J^2 - \beta^2}} dz \right.$$

$$\left. + n^2 A_{2J} \int_0^d E_z^r \Big|_{r = r_1 \text{ or } r_2} \cos(z\sqrt{n^2\beta^2 - \lambda_J^2}) dz \right\}$$

In the light of equation (17), equation (18) vanishes.

Consider the sourceless region V, of Fig. 16 with the fields $\vec{E}$ and $\vec{B}$ existing in the region. The application of equation (7) to the two components $\vec{E}^r$, $\vec{B}^r$ and $\vec{E}_J^G$, $\vec{B}_J^G$ of $\vec{E}$ and $\vec{B}$ with the result of equation (18) yields.

19. $$\frac{Re}{2\mu} \int_{S_1} \hat{r} \cdot (\vec{E}_J^G \times \vec{B}^{*r}) dS_1 = \frac{Re}{2\mu} \int_{S_2} \hat{r} \cdot (\vec{E}_J^G + \vec{B}^{*r}) dS_2$$

$$= \text{constant in r}$$

Since r_1 and r_2 may be independently varied.

The substitution of the explicit expression for E_J^G, allowing βr to become very large and examining the result in a manner similar to that used in deducing that the constant in equation (15) was zero, verifies that equation (19) is zero for all r.

Combining the results of equation equations (18) and (19) verifies equation (5).

It follows that equation 4 becomes

20. $$P = \frac{Re}{2\mu}\left[\int_S \hat{n}\cdot(\vec{E}^r \times \vec{B}^r)dS + \sum_{J=1}^{k}\int_s \hat{n}\cdot(\vec{E}_J^G \times B_J^{G*})dS\right]$$

$$= P^r + P^G$$

This allows the division of the power transferred across a surface, S, surrounding the source into two or more parts and hence to separately compute the powers radiated and that transferred across S by each guided mode.

VII

The Power Radiated by the Dipoles

The time-average power output of the sources may be computed conveniently by one of two methods:

a) the integration of the Poynting's vector over a surface surrounding the source in the far zone: or b) an integration at the source. Both methods lead to the same results. Method b) is preferred for simplicity.

Let use be made of equation (6.7)[22] with $\vec{E}_A = \vec{E}$, $\vec{B}_B = \vec{B}$ and $\vec{P}_B = \vec{P}$, noting as in (6.13) that the polarization, $\vec{P}$, has the form of a constant times a delta-function to obtain:

1. $$P = \frac{Re}{2\mu}\int_S \hat{n}\cdot(\vec{E}\times\vec{B})dS = -\,Re\,\frac{i\omega}{2}\int_V \vec{P}^*\cdot E\,dV$$

$$= Im\,\frac{\omega}{2}\begin{cases} p(z')^* \; E_z(0,z') & \text{Hertzian dipole at } r' = 0,\ z' \neq 0 \\ \frac{p(0)^*}{2} \; E_z(0,0) & \text{Abraham dipole } r' = 0,\ z' = 0 \end{cases}$$

Where S is a surface surrounding the source and V is the volume enclosed by S.

If $E_z(0,z')$ is computed from equations (2.29) to (2.34) by the application of equations (2.8) and (2.9), and substituted in equation (1), and use is made of 'Hospital's Rule for evaluating indeterminate fractions or the well-known expression for the power radiated by an isolated Hertz dipole[23, 24] is utilized, the expressions for P result:

Case A.

$$2.\quad P_{(A)} = \frac{|p_1(z')|^2 \omega \beta^3}{4\pi\varepsilon}\left[\frac{1}{3} + \frac{\cos[2\beta(z'-d)]}{4\beta^2(z'-d)^2} - \frac{\sin[2\beta(z'-d)]}{8\beta^3(z'-d)^3} + \mathrm{Im}\int_0^\infty I\, e^{-2\ell(z'-d)}\, d\lambda\right]$$

Case B.

$$3.\quad P_{(B)} = \frac{|p_2(z')|^2 \omega n \beta^3}{4\pi\varepsilon}\left[\frac{1}{3} + \frac{\sin 2n\beta z'}{8\beta^3 n^3 z'^3} - \frac{\cos 2n\beta z'}{4\beta^2 n^2 z'^2} - \mathrm{Im}\int_0^\infty \frac{I.(\ell m^{-1} - n^{-2}) e^{-md} \cosh^2 mz'}{n^3 \cosh md}\, d\lambda\right]$$

Case C

$$4.\quad P_{(C)} = \frac{|p_2(0)|^2 \omega n \beta^3}{8\pi\varepsilon}\left[\frac{1}{3} - \mathrm{Im}\int_0^\infty \frac{I.(\ell m^{-1} - n^{-2}) e^{-md}}{2n^3 \cosh md}\, d\lambda\right]$$

where:

$$I = \frac{\lambda^3 \quad \beta^{-3}}{\ell + \mu n^{-2} \tanh md}$$

If the integrals are closely examined and integrated wherever possible they are seen to result in:

Case A

$$5.\quad \mathrm{Im}\int_0^{\infty} I\, e^{-2\ell(z'-d)}\,d\lambda =$$

$$\int_0^1 \frac{x^3\,dx\left\{\sqrt{1-x^2}\cos[2\beta(z'-d)\sqrt{1-x^2}]-n^{-2}\sqrt{n^2-x^2}\tan(\beta d\sqrt{n^2-x^2})\sin[2\beta(z'-d)\sqrt{1-x^2}]\right.}{n^{-4}(n^2-x^2)\tan^2(\beta d\sqrt{n^2-x^2}) + 1 - x^2}$$

$$+ \frac{\pi}{\beta^3}\sum_{J=1}^{k} e^{-i\pi/4}\,\lambda_J^2\, e^{-2(z'-d)\sqrt{\lambda_J^2-\beta^2}}\; Q(\lambda_J,\ \beta,\ n,\ d)$$

Case B

$$6.\quad -\mathrm{Im}\int_0^{\infty} \frac{I\cdot(\ell m^{-1} - n^{-2})e^{-md}\cosh^2 mz'\,d\lambda}{n^3\cosh md} =$$

$$-\frac{\sqrt{n^2-1}}{3n} - \frac{\sin(2\beta z'\sqrt{n^2-1})}{4\beta z' n^3} - \frac{\sqrt{n^2-1}}{6n^3}$$

$$+\sqrt{n^2-1}\,\frac{\cos(2\beta z'\sqrt{n^2-1})}{4n^3\beta^2 z'^2} - \frac{\sin(2\beta z'\sqrt{n^2-1})}{8\beta^3 z'^3 n^3}$$

$$+\frac{1}{n^3}\int_0^1 \frac{x^3\,dx\left[\frac{\sqrt{1-x^2}}{\sqrt{n^2-x^2}} - r^{-2}\right]\cos^2(\beta z\sqrt{n^2-x^2})\left[n^{-2}\sqrt{n^2-x^2}\,\tan^2(\beta d\sqrt{n^2-x^2})-\sqrt{1-x^2}\right]}{n^{-4}(n^2-x^2)\tan^2(d\sqrt{n^2-x^2}) + 1-x^2}$$

$$+\frac{\pi}{n^5\beta^3}\sum_{J=1}^{k} \frac{\lambda_J^2 e^{-i\pi/4}\cos^2(z'\sqrt{n^2\beta^2-\lambda_J^2})Q(\lambda_J,\beta,n,d)}{\cos^2(d\sqrt{n^2\beta^2-\lambda_J^2})}$$

Case C

$$7. \qquad -\operatorname{Im}\int_0^{\infty} \frac{I(\ell_m^{-1}-n^{-2})e^{-md}\,d\lambda}{2n^3\cosh md} =$$

$$-\frac{(2n^2+1)}{6n^3}\sqrt{n^2-1}+\frac{1}{2n^3}\int_0^1 \frac{x^3\,dx\left[\frac{\sqrt{1-x^2}}{\sqrt{n^2-x^2}}-n^2\right]\left[n^{-2}\sqrt{n^2-x^2}\tan^2(\beta d\sqrt{n^2-x^2})-\sqrt{1-x^2}\right]}{n^{-4}(n^2\beta^2-x^2)\tan^2(\beta d\sqrt{n^2-x^2})+1-x^2}$$

$$+\frac{\pi}{2n^5\beta^3}\sum_{J=1}^{k}\frac{\lambda_J^2 e^{-i\pi/4}Q(\lambda_J,\beta,n,d)}{\cos^2(d\sqrt{n^2\beta^2-\lambda_J^2})}\,,$$

where $Q(\lambda_J,\beta,n,d)$ is defined in section III.

If method (a), in conjunction with equations (4.20), (4.1) to (4.10) were used to compute P^G, it would be found that this yields exactly the last term in equations (5-7). Hence, the terms in the summations when substituted in equations (2-4) are the total powers transferred into the guided modes from the dipoles. It is to be noted that it is necessary to prove that the power can be subdivided as in (4.20) before the two divisions can be compared.

As was previously observed the total power allotted to a guided mode (the summations terms in equations (5-7)) is not acquired by the mode until βr becomes infinite. To a good approximation this is true for βr greater than the values of Fig. 5. To this approximation, then, equations (2-7) may be given the following interpretation according to equation (4.20). P is the total power transferred across S.

$$P^G = \sum_{J=1}^{k} P_J^G$$

is equal to the summation terms in equations (2-7) and is equal to the power transferred across S by the guided modes, where S has a minimum radius βR which is greater than the values of βr in Fig. 5. P^r is equal to the remaining terms of equations (2-7) and is equal to the power transferred across S by the compensating waves.

$$P = P^r + \sum_{J=1}^{k} P_J^G$$

If equations (2) and (3) are evaluated at $z' = d+$ and $z' = d-$, respectively, it turns out that the powers are identical if $p_2(d-) = n^2 p_1(d+)$. This verifies the previous result.

Figures 18 and 19 contain curves of $\frac{4\pi\epsilon P}{|p^2|\omega\beta^3}$ as a function of dipole height, $\beta z'$, for $n^2 = 2.54$, for two thicknesses of dielectric, $\beta d = 0.15\pi$ and $n\pi/4$. The integrals in equations (5-7) were computed by numerical integration. Comparison curves with

$\beta d = 0$ are given.

The discontinuities at $\beta z = \beta d$ in Figs. 18 and 19 are due to the above-mentioned discontinuities of the magnitudes of the sources. The total powers are seen to decrease with $\beta z'$ in the dielectric. The slight humps in this region are seen to occur at the maxima in Figs. 20 and 21. For $\beta z' > \beta d$ the powers fluctuate around the values for $\beta z' = 0$. Both converge upon $\frac{1}{3}$ as $\beta z'$ approaches large values, indicating that the coupling to the guided modes and image fields approaches zero for large $\beta z'$.

Figures 20 and 21 contain curves of P^G / P^r versus dipole height, $\beta z'$, for the same βd's and n as Figs. 18 and 19. Figures 20 and 21 are seen to have maxima near the dielectric and conductor surfaces and to decrease uniformly with $\beta z'$ and $\beta z' \geq \beta d$. The minimum between the two maxima agrees with the minimum in Figs. 18 and 19 for $\beta d = 0$. The two maxima correspond to the two methods of feeding a balanced two-wire transmission line: (a) a concentrated generator in the terminal piece, or (b) two equal concentrated generators of opposite polarities in the two wires at the same cross-section.

For the smaller $\beta z'$, the large magnitudes of the ratios of Fig. 20 and 21 indicate that an overwhelming portion of the power radiated by the dipole is transferred to the guided or surface waves. In these cases the nomenclature of compensating wave for the radiated component of the field is a preferred one.

VIII

The Attenuation Constant of a Guided Mode

Due to the Finite Conductivity of the Ground Plane

The attenuation constant, α_J, for $\beta r >> 1$, of the J^{th} guided mode due to a large but finite conductivity of the ground plane is derived.

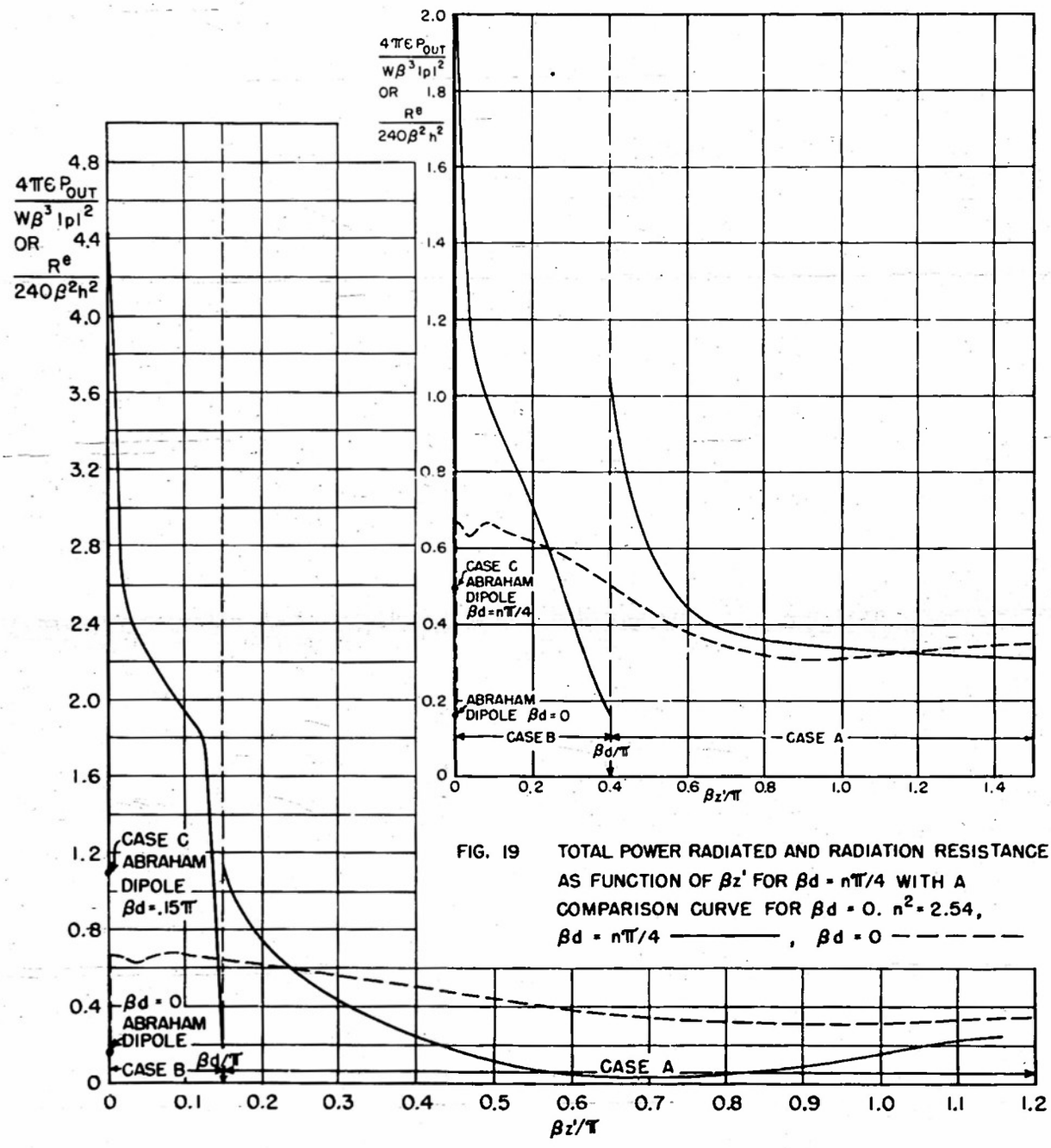

FIG. 19 TOTAL POWER RADIATED AND RADIATION RESISTANCE AS FUNCTION OF $\beta z'$ FOR $\beta d = n\pi/4$ WITH A COMPARISON CURVE FOR $\beta d = 0$. $n^2 = 2.54$, $\beta d = n\pi/4$ ——— , $\beta d = 0$ — — — —

FIG. 18 TOTAL POWER RADIATED AND RADIATION RESISTANCE AS A FUNCTION OF $\beta z'$ FOR $\beta d = 0.15\pi$ WITH A COMPARISON CURVE FOR Bd = 0

n = 2.54 $\beta d = .15\ \pi$ —— $\beta d = 0$ ---

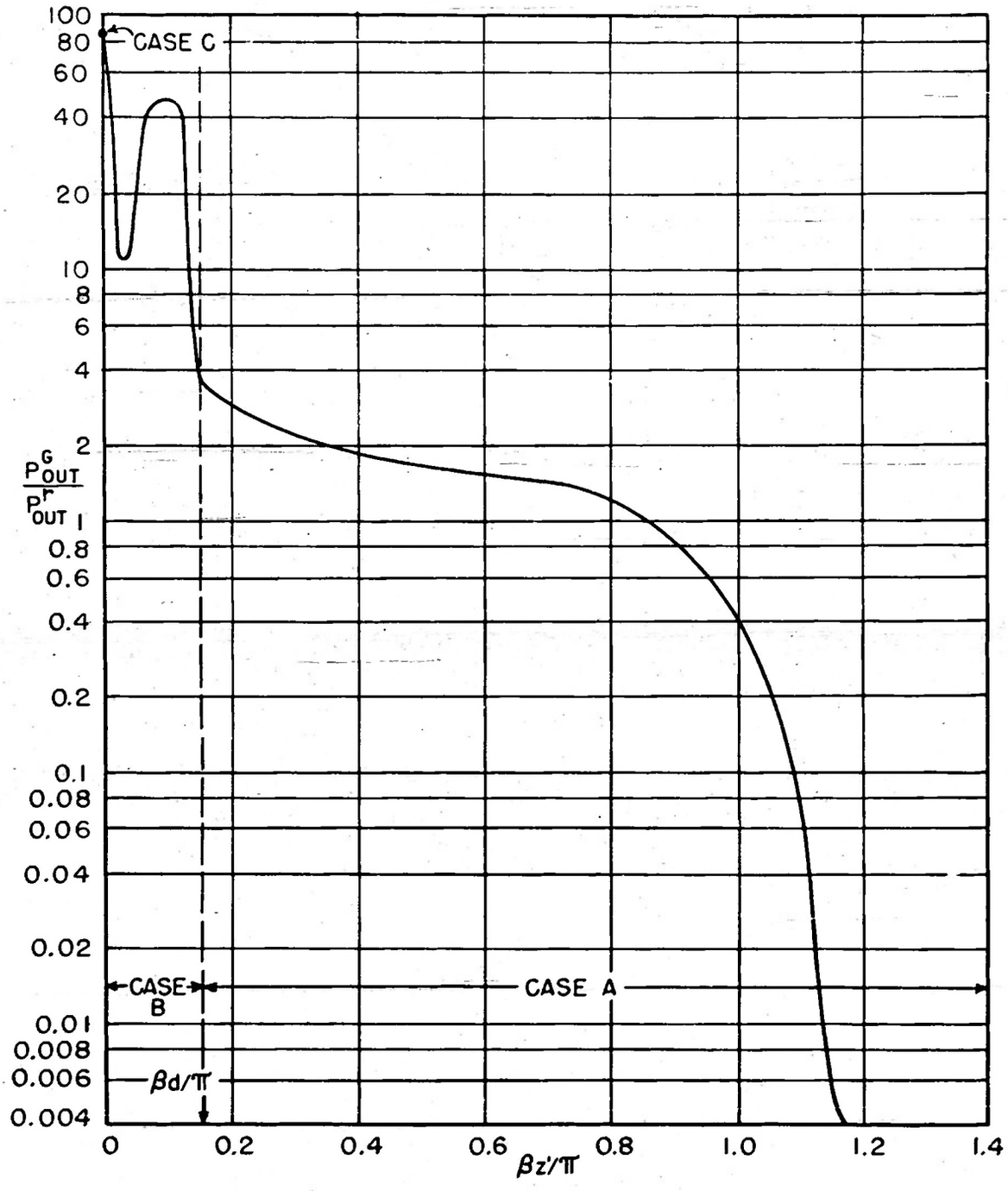

FIG. 20 P^G_{OUT}/P^r_{OUT} AS A FUNCTION OF $\beta z'$ FOR $\beta d = 0.15\pi$ $n^2 = 2.54$ THIS INCLUDES CASES A, B AND C AS $\beta z'$ VARIES.

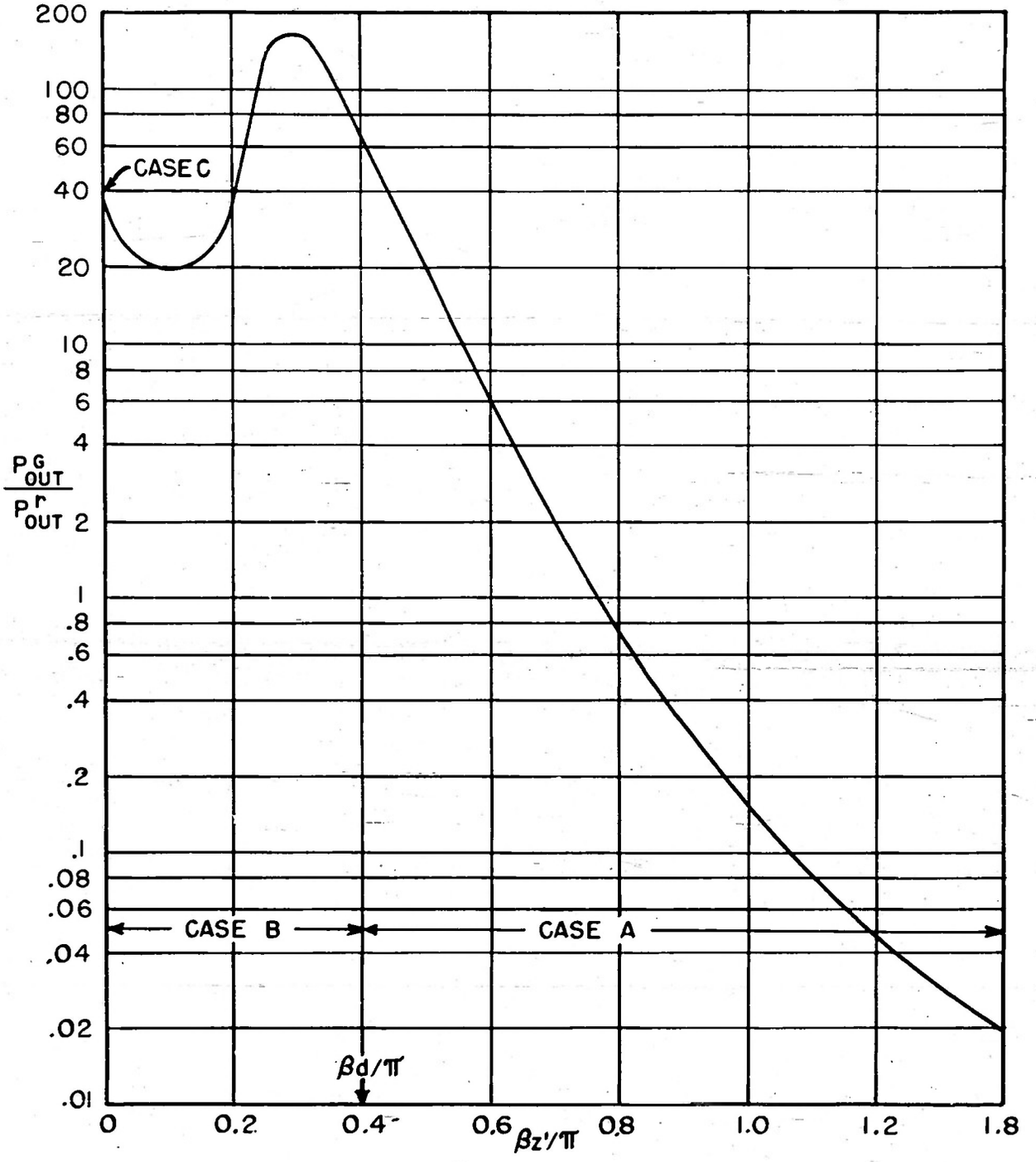

FIG. 21 P^G_{OUT}/P^r_{OUT} AS A FUNCTION OF $\beta z'$ FOR $\beta d = n\pi/4$, $n^2 = 2.54$ THIS INCLUDES CASES A, B AND C AS $\beta z'$ VARIES

Use is made of the following formula:*

1. $$\alpha_J = -\frac{1}{2}\frac{\partial P_J^G/\partial r}{P_J^G}$$

If the following procedure is followed equation (2) will result for cases A, B, and C.

a) Assume the fields are those of equations (4.1) - (4.10) except for a small component $Er_J^{FG}(r,o)$

b) Assume P_J^G is that of equations (7.2) - (7.7).

c) Set $H_{\theta J}^G(r,o) = -l_{rJ}(r,o) \doteq -Er(r,o)/z_S$.
Where: $l_{rJ}(r,o)$ is a quasi-surface current.

$$z_S = (1-i)\sqrt{\frac{\omega\mu}{2\sigma}}$$

d) Compute

$$-\frac{\partial P_J^G}{\partial r} = \frac{1}{2}\,\mathrm{Re}\int_0^{2\pi} z_S\left|l_{rJ}(r,o)\right|^2 r\,d\theta$$

$$= \frac{R_S}{2}\int_0^{2\pi}\left|H_{\theta J}(r,o)\right|^2 r\,d\theta$$

e) Substitute e and b in equation 1

$$2.\ \alpha_J = \frac{n^2\beta^2}{\lambda_J\sqrt{2\omega\sigma\mu}}\cdot\frac{\sqrt{\lambda_J^2-\beta^2}\left[(\beta^2-n^{-2}\lambda_J^2)+n^2(\lambda_J^2-\beta^2)\right]}{\left\{\beta^2(n^2-1)+d\sqrt{\lambda_J^2-\beta^2}\left[(\beta^2-n^{-2}\lambda_J^2)+n^2\sqrt{\lambda_J^2-\beta^2}\right]\right\}}$$

For cases A, B, and C.

---

*Lecture notes of R. D. Kodis and E. T. Kornhauser at Harvard University.

Figure 22 contains a plot of $\frac{\sqrt{2\omega\sigma\mu}}{n^2\beta^2}\alpha_J$ as βd varies, for $n^2 = 2.54$, and $.10\pi \leq \beta d \leq 1.6\pi$, for the existing modes 1 and 2. It is to be noted that the attenuation constant for each mode increases to a maximum and then decreases uniformly with increasing βd. These maximum values of attenuation appear approximately halfway between the cutoff thicknesses. The attenuation constants for the higher modes are lower than those for the lower modes since the factor d appears in the denominator of (2) and the higher modes appear with larger βd.

IX

The Radiation Resistance

The radiation resistance may be computed by referring it to the uniform current on the dipole, $I(z')$.

$$(1) \qquad R^e = \frac{2P}{|I(z')|^2}$$

where $I(z') = -\frac{i\omega p(z')}{2h}$ for both the Abraham and Hertz dipoles and h = the half-length of the Hertz dipole = the length of the Abraham dipole.

Hence:

$$(2) \qquad \frac{R^e}{240\beta^2 h^2} = \frac{4\pi\varepsilon P}{\omega\beta^3 |p(z')|^2}$$

This is plotted with P in Figs. 18 and 19.

Acknowledgements

The author wishes to thank Professor R. W. P. King and Dr. Tetsu Morita for their advice and encouragement. He also wishes to express his gratitude to Miss Mary Tynan for carrying out the extensive computations.

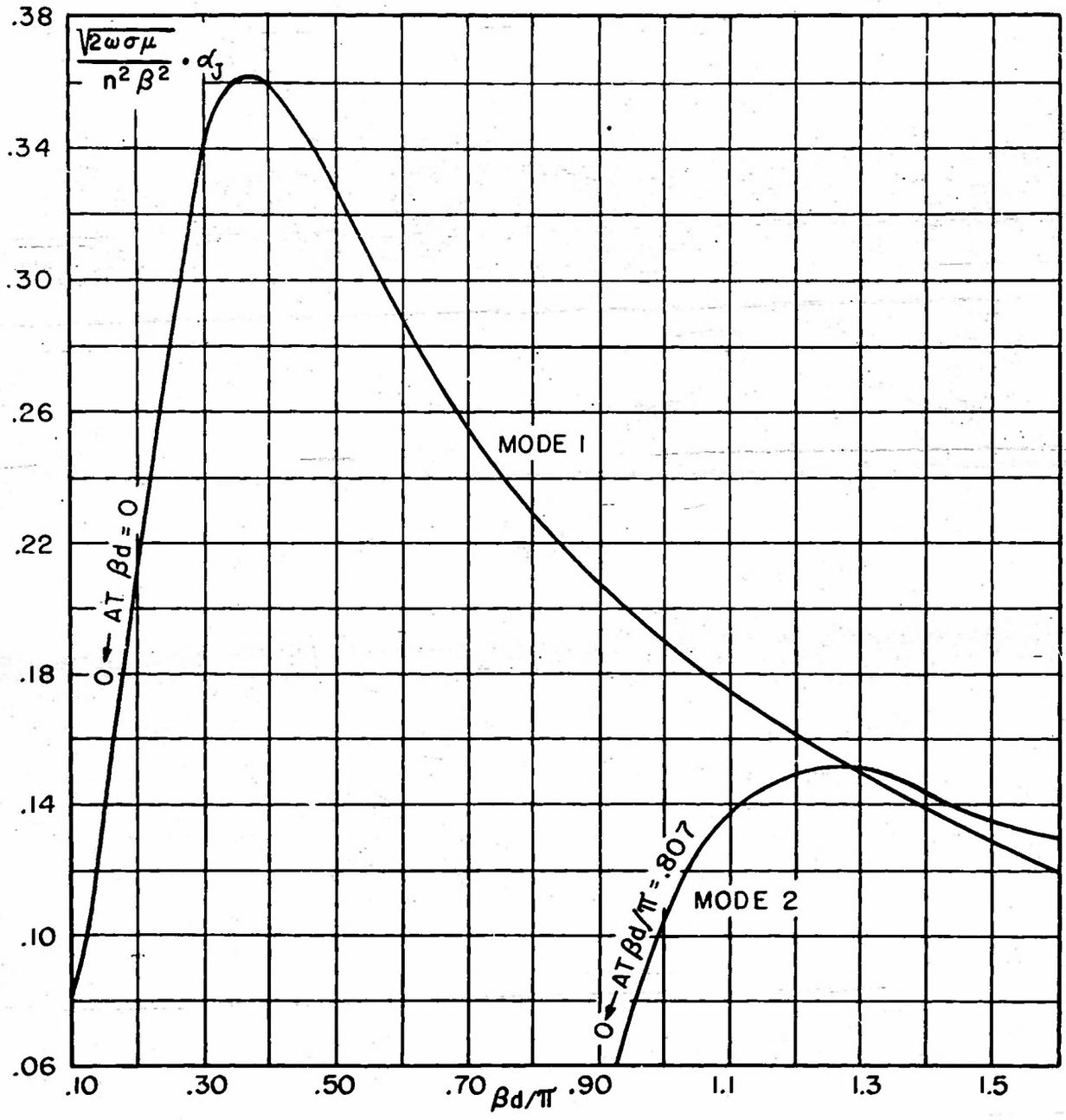

FIG. 22 ATTENUATION OF A SURFACE MODE DUE TO A LARGE BUT FINITE CONDUCTIVITY σ OF THE GROUND PLANE AS A FUNCTION OF DIELECTRIC THICKNESS βd.

$n^2 = 2.54$ $\qquad 0.10\pi \leq \beta d \leq 1.6\pi$

Appendix A

To illustrate the type of integration performed to yield equations (3.5), (3.6), (3.7) and (3.9), consider the integral in (2.29), after it has been transformed by (3.1), to be integrated over W_1 of Fig. 3.

$$(A\text{-}1) \qquad I = \frac{1}{2}\int_0^\infty \frac{e^{-\ell(z+z'-2d)}}{\ell+mn^{-2}\lambda\tanh md} H_o^1(\lambda r)\lambda d\lambda$$

It is convenient to make the following substitution:

$$(A\text{-}2) \qquad R''\sin\theta_1 = z + z' - 2d; \quad R''\cos\theta_1 = r \qquad \text{Fig. 2a}$$

$$(A\text{-}3) \qquad \lambda = \beta\sin\alpha; \qquad \sqrt{\beta^2 - \lambda^2} = \beta\cos\alpha$$

The Riemann sheet of interest in the λ-plane of Fig. 3 transforms into the curved strip in the α-plane, Fig. A-1. The transformation of the branch cuts (which are not branch cuts in the α-plane) are defined by sin x cosh y=1. Under the assumption that $\beta R''\cos\theta_1 >> 1$ so that H_o^1 may be replaced by its asymptotic form for large argument, and substituting (A-2) and (A-3) in (A-1), (A-1) becomes:

$$(A\text{-}4) \qquad I = -\frac{e^{-i\pi/4}\beta^2}{4\pi}\int_{W_1}\sqrt{\frac{2\sin\alpha}{\pi R''\beta\cos\theta_1}}\frac{\cos\alpha\, e^{i\beta R''(\cos\alpha\sin\theta_1+\sin\alpha\cos\theta_1)}\, d\alpha}{[i\beta\cos\alpha+\beta n^{-2}\sqrt{n^2-\sin^2\alpha}\tan(\beta d\sqrt{n^2-\sin^2\alpha})]}$$

This is of the proper form for an integration by the method of steepest descents,[10, 12] when $R'' >> d$.

The saddle-point is at $\alpha = \pi/2-\theta$.

The path of steepest descent, W, is defined by $\sin(x + \theta_1)\cosh y = 1$ (Fig. A-1).

If the assumption is made that the poles are not near enough to the $\alpha = \pi/2$ to affect the integrand before the exponential

factor has attenuated it to negligible value*,[12] then the integration over W results in:

$$(A\text{-}5) \quad -\frac{i\beta e^{i\beta R''}}{4\pi\beta''} \frac{\sin\theta_1}{i\beta\sin\theta_1 + \beta n^{-2}\sqrt{n^2-\cos^2\theta_1}\tan(\beta d\sqrt{n^2-\cos^2\theta_1})}$$

and it may be observed that:

$$(A\text{-}6) \quad I = \int_{W_1} \ldots d\alpha = -\int_{W} \ldots d\alpha + 2\pi i \sum \text{Residues enclosed by } W \text{ and } W_1.$$

When W passes through a pole, one-half the residue is included[10, 12] as a contribution to the integration. If the pole is included between W and W_1, the whole residue is contributed to (A-6), while if the pole is excluded by path $W\text{-}W_1$, there is no contribution from it.

It is relatively easy to verify that W passes through a pole when $\theta_1 = \cos^{-1}\beta/\lambda_J$, and from this relationship the coefficients $A_J(\theta_1)$ of the residue waves arise. The residue terms are evaluated by well-known methods.

The rapid decrease of the coefficient $A_J(\theta_1)$ at its critical value is due to the fact that for large βR the path passes very rapidly through the pole as θ_1 varies.

The results obtained thus far have been restricted to $\beta R'' \cos\theta_1 >> 1$ by virtue of the assumption that the Hankel function could be replaced by its asymptotic form. Actually, the restriction is less strict for a good approximation and it may be modified to $\beta R'' >> 1$ and $(\beta R'' \cos\theta_1)^2 >> 1$. This leaves only a small region near $\theta_1 = \pi/2$ where the results developed are not valid. The restrictions may be further modified by the following:

- - - - - - -

*See Appendix B for the exact condition.

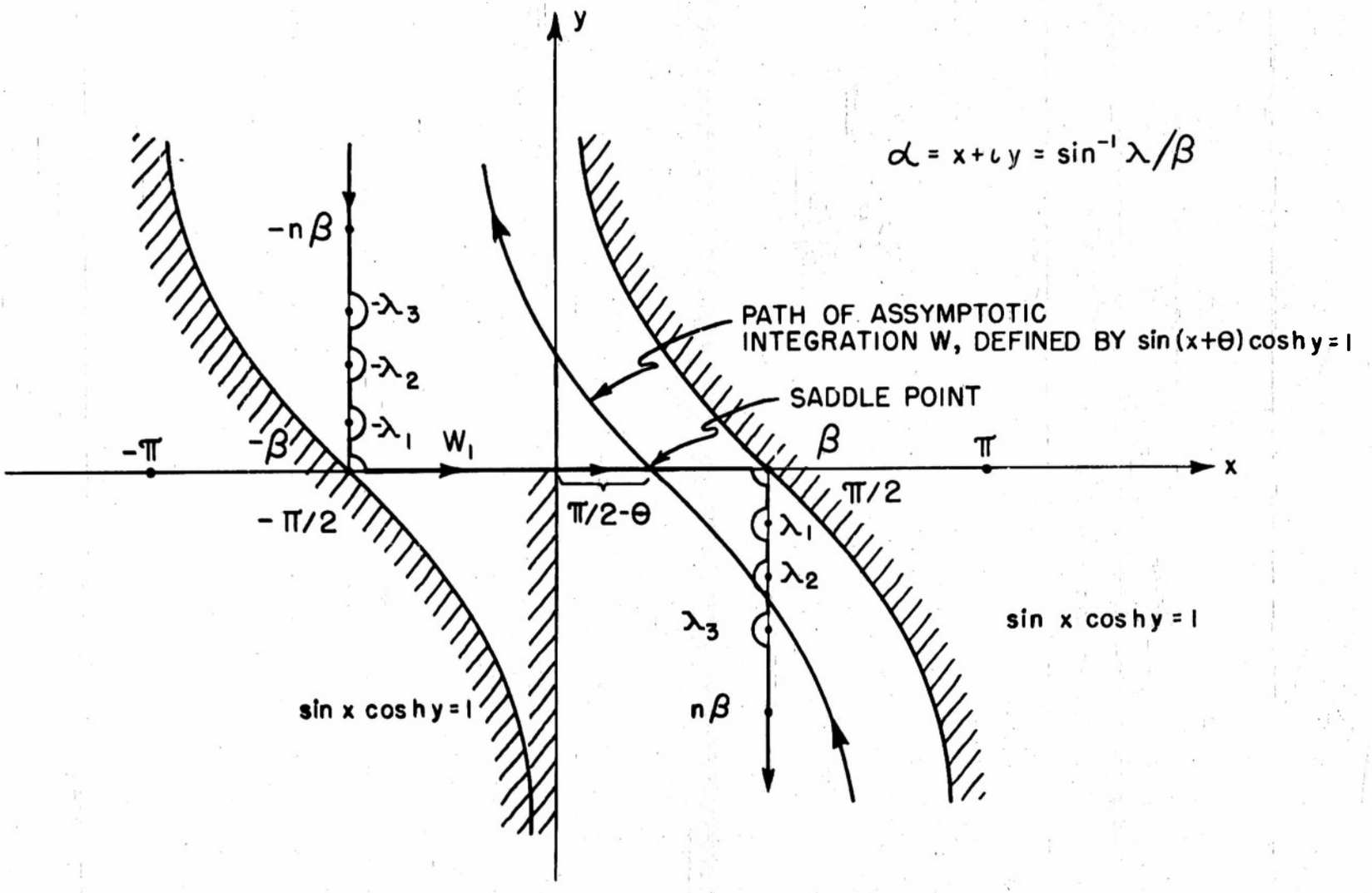

FIG. A-1 PATH OF INTEGRATION IN THE $\alpha = \sin^{-1} \lambda/\beta$ PLANE

Consider (2.29) for $r = o$, $\theta_1 \doteq \pi/2$, $\beta R'' \doteq \beta z >> 1$

$$(A\text{-}7) \qquad I\Big|_{r=o} = \int_0^\infty \frac{e^{-\ell(z+z'-2d)}}{\ell + mn^{-2}\tanh md}\, \lambda d\lambda$$

Performing the same transformations, (A-2) and (A-3), and integrating over half the path W (the part on and below the x-axis of Fig. A-1) in the α-plane, the following is obtained:

$$(A\text{-}8) \qquad I\Big|_{r=o} = \frac{i}{2\pi} \frac{e^{i\beta(z+z'-2d)}}{(z+z'-2d)(i+n^{-1}\tan\beta nd)},$$

where there are no residue terms since $\beta z >> 1$ and $\theta_1 = \pi/2 > \cos^{-1}\beta/\lambda_J$ ($A_J(\theta) = 0$).

It is seen that $I\Big|_{r=o} = \lim_{\theta_1 = \pi/2} I\Big|_{\text{eq. A-6}}$

It is therefore a reasonable assumption that equation (A-6) is valid for all θ_1, $0 \leq \theta_1 \leq \pi/2$, $\beta R'' >> 1$.

The integrations of equations (2-30), (2.31), and (2.33) are performed in a similar manner.

Appendix B

As an illustrative example of the application of the method of B. L. Van Der Waerden[13] to the integration of equations (2.32) and (2.34), consider the following integral, obtained by applyiing (3.1) to (2.32).

$$(B\text{-}1) \qquad I = -\frac{1}{4\pi} \int_{-\infty}^{\infty} \frac{(\ell - mn^{-2})\cosh mz' \cosh mz \; e^{-md\lambda} H_o^1(\lambda r) d\lambda}{m(\ell \cosh md + mn^{-2} \sinh md)}$$

W_2

Since the integrand of (B-1) has two extra branch cuts, (3) and (4) in Fig. 3, at $\lambda = \pm n\beta$, and one of these intersects the path of steepest descent for the integrand in (B-1) if the method of steepest descents, Appendix A, is used, the integration by the method of steepest desents is complicated. The Van Der Waerden method contains a systematic procedure for integrating around branch cuts.

In order to put (B-1) in Van der Waerden's form the following transformation is performed.

$$(B\text{-}2) \qquad \lambda = i\mu$$

Substitute the asymptotic representation for large λr for $H_o^1(\lambda r)$.

The transformed $\mu = -i\lambda$ - plane is shown in Fig. B-1 where (1), (2), (3), (4), and (5) are the branch cuts that appear in the λ - plane, Fig. 3.

Then:

$$(B\text{-}3) \qquad I = \int_{W_2} W e^{-r\mu} dv \qquad \text{for } \beta r >> \beta d,$$

Where r corresponds to Van Der Waerden's λ.

In the μ-plane the saddle-point of the μ-plane becomes another branch point.[13] In this case there is no added complication

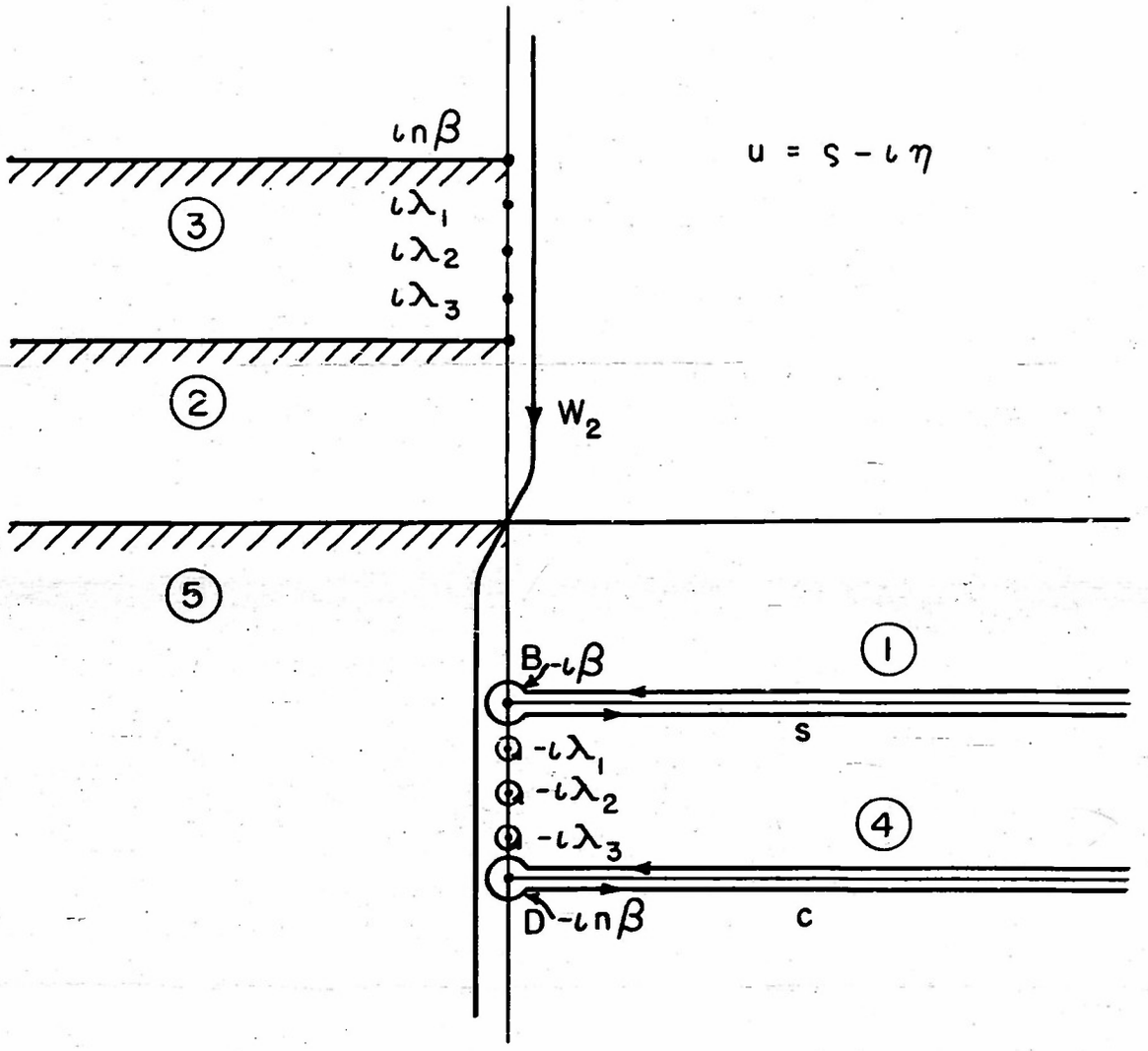

FIG. B-1 PATHS OF INTEGRATION FOR CASE B-2, C-2 IN THE $u = -\iota\lambda$ PLANE

because this added branch point is coincident with the one at $\mu = -i\beta$.

For large r and for a contour shifted far to the right in Fig. B-1, the integral reduces to integrations over the branch cuts and poles. The former yield rapidly converging series for large λr and for poles not to close to the branch points.

Performing the integrations exactly as Van Der Waerden does, the following is obtained:

$$(B\text{-}4) \qquad I = 2\pi i \sum_{J=1}^{k} \text{Residue} - \frac{1}{2\pi r} e^{in\beta r} + O(r^{-2}),$$

where $O(r^{-2})$ indicates a term of order r^{-2} and yields an estimate of the error.

The residue are computed in the usual way and are modified by equation (3.2) to yield the summation terms of (3.8).

If in equation (2.32) it is assumed that

$$\left.\begin{matrix} \beta z' \\ \text{and} \\ \beta z \end{matrix}\right\} \leq \beta d << \beta r,$$

then $\beta R^V \doteq \beta R' \doteq \beta r$ and equation (3.8) is obtained.

It has been assumed that the poles are not too near to the branch points. An estimate of not too near is a result of the Van Der Waerden method. It is:

$$(B\text{-}5) \qquad \left.\begin{matrix} a) \quad e^{-r|\beta-\lambda_1|} \\ \text{and} \\ b) \quad e^{-r|n\beta-\lambda_k|} \end{matrix}\right\} << O(r^{-2}) << O(r^{-1})$$

If the integrations in Appendix A had been performed by the method in Appendix B, the definition of the pole being not too near the branch point would be found to be (B-5a). Hence equation (B-5a) and (B-5b) are necessary restrictions for all the equations (3.5) - (3.10).

References

1. Nathan Marcuvitz, "Guided Wave Concept in Electromagnetic Theory," Research Report R-269-52, P.I.B.-208, ONR, May 14, 1952. Polytechnic Institute of Brooklyn, Microwave Research Institute, pp. 1-5.

2. A. Sommerfeld, Partial Differential Equations in Physics, Academic Press, New York, 1949, pp. 246-257.

3. J. A. Stratton, Electromagnetic Theory, McGraw-Hill, New York, 1941, pp. 573-583.

4. S. Attwood, "Surface Wave Propagation over a Coated Plane Conductor," J. Appl. Phys. 22, 504-509 (1951).

5. Frank-Mises, Differentialgleichungen der Physik, Vol. II, Chap. XIX, Sec. 5, Frederich Vieweg und Sohn, Brunswick, Germany, 1935.

6. R. W. P. King, Electromagnetic Engineering, Vol. II, McGraw-Hill, New York, 1945, p. 232.

7. J. A. Stratton, supra, p. 371.

8. Op. cit., pp. 486-487.

9. Op. cit., pp. 575-576.

10. C. T. Tai, "The Effect of a Grounded Slab on Radiation from a Live Source," J. Appl. Phys. 22, 405-414 (1951).

11. J. A. Stratton, supra, pp. 584-585.

12. Karp and Sollfrey, "Diffraction by a Dielectric Wedge," Research Report No. EM-23, Mathematical Research Group, New York University, October, 1950, pp. 19-22, 31-36.

13. B. L. Van Der Waerden, "On the Method of Saddle Points," Applied Scientific Research, Vol. B-2, No. 7, Martinus Nijhoff, The Hague, 1951, pp. 43-45.

14. Jahnke and Emde, Tables of Functions, Dover, New York, pp. 134,136.

15. R. W. P. King, supra, pp. 268-269, 276-278.

16. G. Goubau, "Surface Waves and Their Application to Transmission Lines," J. Appl. Phys. 21, 1119-1128 (1950).

17. G. Goubau, "Single Conductor Surface-Wave Transmission Lines," Proc. I.R.E. 39, 619-624 (1951).

18. G. Goubau, "On the Excitation of Surface Waves," Proc. I.R.E. 40, 865-868 (1952).

19. G. Goubau, "Über die Zennecksche Bodenwelle," Zeit. Ang. Physik, Vol. 3, March, 1951, pp. 103-107.

20. R. W. P. King, supra, pp. 220-221.

21. J. A. Stratton, supra, p. 479.

22. R. W. P. King, supra, p. 221.

23. J. A. Stratton, supra, pp. 435-437.

24. R. W. P. King, supra, pp. 296-297.

Additional Reports Issued by Cruft Laboratory

(under Contract N5ori-76)

in the Field of Electromagnetic Radiation

No.

2 D. D. King, "Measured Impedance of Cylindrical Dipoles," 1946. J. Appl. Phys., Oct. 1946.

6 D. D. King, "Impedance Measurements on Transmission Lines," 1946. Proc. I.R.E., May 1947.

8 B. C. Dunn, Jr. and R. W. P. King, "Currents Excited on a Conducting Plane...," 1947. Proc. I.R.E., Feb. 1948.

11 D. D. King et al, "Bolometer Amplifier for Minimum Signals," 1947. Electronics, Feb. 1948.

12 C. T. Tai, "Theory of Coupled Antennas," 1947. Part I Proc. I.R.E., April 1948; Part II, ibid, Nov. 1948.

16 Tung Chang, "Impedance Measurements of Antennas Involving Loop and Linear Elements," 1947.

18 C. T. Tai, "Propagation of Electromagnetic Waves from a Dissipative Medium to a Perfect Dielectric," 1947.

20 R. W. P. King, "Graphical Representation of the Characteristics of Cylindrical Antennas," 1947.

22 C. H. Papas and R. W. P. King, "Radiation Resistance of End-Fire Collinear Arrays," 1947. Proc. I.R.E., June 1948.

23 R. W. P. King, "Field of Dipole with Tuned Parasite at Constant Power," 1947. Proc. I.R.E., July 1948.

25 J. V. Granger, "Low-Frequency Aircraft Antennas," 1947.

27 C. H. Papas and R. W. P. King, "Surface Currents on a Conducting Plane...," 1948. J. Appl. Phys., Sept. 1948.

28 C. T. Tai, "Reflection and Refraction of a Plane Electromagnetic Wave...," 1948.

32 C. H. Papas and R. King, "Currents on the Surface of an Infinite Cylinder," 1948. Quart. Appl. Math., Jan. 1949.

35 P. Conley, "Impedance Measurements with Open-Wire Lines," 1948. J. Appl. Phys., Nov. 1949.

39 S. B. Cohn, "Theoretical and Experimental Study of a Waveguide Filter Structure," 1948.

40 C. T. Tai, " Reflection of Plane Electromagnetic Waves from Perfectly Conducting Grounded Half-Cylinder," 1948.

41 R. W. P. King, "Theory of Antennas Driven from a Two-Wire Line," 1948. J. Appl. Phys., Sept. 1949.

42 J. V. Granger, "Note on Broad-Band Impedance Characteristics of Folded Dipoles," 1948.

43 D. G. Wilson and R. King, "Measurement of Antenna Impedance Using Receiving Antenna," 1948.

44 E. Hallen, "Properties of Long Antennas," 1948. J. Appl. Phys., Dec. 1948.

46 E. Hallén, " Admittance Diagrams for Antennas...," 1948.

47 C. T. Tai, "On the Theory of Biconical Antennas," 1948. J. Appl. Phys., Dec. 1948.

48. K. Tomiyasu, "Problems of Measurement on Two-Wire Lines with Application to Antenna Impedance," 1948. Condensed version, J. Appl. Phys., Oct. 1949.

49 E. Hallén, "Traveling Waves and Unsymmetrically Fed Antennas, 1948.

50 D. D. King, "Measurement and Interpretation of Antenna Scattering," 1948.

52 C. H. Papas and R. King, "Input Impedance of Wide-Angle Conical Antennas," 1948. Proc. I.R.E., Nov. 1949.

53 D. K. Reynolds, "Surface-Current and Charge Measurements on Flat Metal Sheets," 1948.

55 C. T. Tai, "Study of the EMF Method," 1948. J. Appl. Phys., July 1949.

56 T. W. Winternitz, "The Cylindrical Antenna Center-Driven by a Two-wire Open Transmission Line," 1948. Quart. Appl. Math., 1949.

58 C. H. Papas, "On the Infinitely Long Cylindrical Antenna," 1948. J. Appl. Phys., May 1949.

61 C. H. Papas, "Radiation from a Transverse Slot in an Infinite Cylinder," 1948. J. Math. and Phys., Jan. 1950.

63 J. V. Granger and N. G. Altman, "Full-Scale Aircraft Antenna Measurements," 1949.

66 T. Morita, "Measurement of Current and Charge Distributions on Cylindrical Antennas," 1949. Proc. I.R.E., Aug. 1950.

67 T. Morita and C. E. Faflick, "Measurement of Current Distributions along Coupled Antennas...," 1949.

69 J. E. Storer and R. King, "Radiation Resistance of a Two-Wire Line," 1949.

70 J. V. Granger, "Shunt-Excited Flat-Plate Antennas...," 1949. Proc. I.R.E., March 1950.

71, 72, 73 B. C. Dunn, Jr., "Microwave Field Measurements," I (with R. King), II and III, 1949.

74 R. King and K. Tomiyasu, "Terminal Impedance and Generalized Two-Wire Line Theory," 1949. Proc. I.R.E., Oct. 1949.

75 C. T. Tai, "Application of a Variational Principle to the Study of Biconical Antennas," 1949.

76 C. H. Papas, "Radiation from a Circular Diffraction Antenna," 1949.

77 C. T. Tai, "On Radiation and Radiating Systems in the Presence of a Dissipative Medium," 1949.

78 J. V. Granger and T. Morita, "Current Distribution on Aircraft," 1949.

81 K. Tomiyasu, "Loading and Coupling Effects of Standing-Wave Detectors," 1949. Proc. I.R.E., Dec. 1949.

83 C. H. Papas, "Diffraction by a Cylindrical Obstacle," 1949. J. Appl. Phys., April 1950.

84 R. King, "Theory of N Coupled Parallel Antennas," 1949. J. Appl. Phys., Feb. 1950.

86 K. Tomiyasu, "Unbalanced Terminations on a Shielded-Pair Line," 1949.

91 R. King, "Theory of Collinear Antennas," 1949.

92 C. H. Papas and R. King, "Radiation from Wide-Angle Conical Antennas...," 1949. Proc. I.R.E., Nov. 1949.

93 R. King, "Asymmetrically Driven Antennas and the Sleeve Dipole," 1949.

94 T. Morita, E. O. Hartig, and R. King, "Measurement of Antenna Impedance...," (Supplement to T. R. 43), 1949.

95 C. P. Hsu, "Theory of Helical Waveguides and Helical Radiators," 1950.

96 R. King, "Theory of V-Antennas," 1950.

98 D. J. Angelakos, "Current and Charge Distributions on Antennas and Open-Wire Lines," 1950.

100 H. Levine and C. H. Papas, "Theory of the Circular Diffraction Antenna," 1950.

101 J. E. Storer, "Variational Solution to the Problem of the Symmetrical Cylindrical Antenna," 1950.

105 R. D. Kodis, "An Experimental Investigation of Microwave Diffraction," 1950.

107 E. O. Hartig, "Circular Apertures and their Effects on Half-Dipole Impedances," 1950.

108 E. O. Hartig, "A Study of Coaxial-Line Discontinuities Using a Variational Method," 1950.

146 C. Moritz, "The Coupled Receiving Antenna, I.," 1952.

147 C. Moritz, "The Coupled Receiving Antenna, II.," 1952.

148 C. H. Papas and D. B. Brick, "Radiation of the Boss Antenna," 1952.

149 J. Sevick and J. E. Storer, "A General Theory of Plane-Wave Scattering from Finite Conducting Obstacles with Application to the Two-Antenna Problem," 1952.

150 J. Sevick "Experimental and Theoretical Results on the Back-Scattering Cross Section of Coupled Antennas," 1952.

151 J. Sevick, "An Experimental Method of Measuring Back-Scattering Cross Sections of Coupled Antennas," 1952.

152 J. E. Storer "Wave Propagation in a Two-Dimensional Periodic Medium," 1952.

153 R. V. Row, "Microwave Diffraction Measurements in a Parallel-Plate Region," 1952.

154 R. King, "An Alternative Method of Solving Hallén's Integral Equation and its Application to Antennas near Resonance," 1952.

159 L. S. Sheingold, "The Susceptance of a Circular Obstacle to an Incident Dominant Circular-Electric Wave," 1952.

160 J. E. Storer, L. S. Sheingold, and S. Stein, "A Simple Graphical Analysis of Waveguide Junctions," 1952.

162 T. Morita and L. S. Sheingold, "A Coaxial Magic-T," 1952.

163 "On the Diffraction of Electromagnetic Waves by Annular, Elliptical and Rectangular Apertures," C. Huang, February 1953.

166 "Circumferential Gap in a Circular Waveguide Excited by a Dominant Circular-Electric Wave," L. S. Sheingold and J. E. Storer, March 1953.

170 "Electromagnetic Scattering from Two Parallel Conducting Circular Cylinders." R. V. Row, May 1953.

173 "A Tabulation of Fresnel Integrals," R. Turner and A. Downey, May 1953.

Antenna

D I S T R I B U T I O N

2	Office of Naval Research (427) Navy Department Washington 25, D. C.
1	Office of Naval Research (460) Navy Department Washington 25, D. C.
1	Chief, Bureau of Ordnance (Re4f) Navy Department Washington 25, D. C.
1	Chief, Bureau of Ships (810) Navy Department Washington 25, D. C.
1	Chief, Bureau of Ships (833) Navy Department Washington 25, D. C.
1	Chief, Bureau of Aeronautics (EL-51) Navy Department Washington 25, D. C.
1	Chief of Naval Operations (Op-413) Navy Department Washington 25, D. C.
1	Chief of Naval Operations (Op-20) Navy Department Washington 25, D. C.
1	Chief of Naval Operations (Op-32) Navy Department Washington 25, D. C.
9	Naval Research Laboratory (2027) Bellevue, D. C.
1	Naval Research Laboratory (2020) Bellevue, D. C.
1	Naval Research Laboratory (3480) Bellevue, D. C.
1	Naval Ordnance Laboratory White Oak Maryland
2	U. S. Naval Electronics Laboratory San Diego 52, California

1	Naval Air Development Center (AAEL) Johnsville Pennsylvania
1	U. S. Navy Underwater Sound Laboratory New London Connecticut
	U. S. Navy Office of Naval Research Branch Offices:
2	Boston
1	New York
1	Chicago
1	San Francisco
1	Pasadena
3	U. S. Navy Office of Naval Research U. S. Navy 100, Fleet Post Office New York, N. Y.
1	Librarian U. S. Naval Post Graduate School Monterey, California
1	U. S. Coast Guard (EEE) 1300 E Street, N. W. Washington, D. C.
1	Research and Development Board Pentagon Building Washington 25, D. C.
1	National Bureau of Standards Department of Commerce Washington, D. C. Attention: Dr. N. Smith
1	Naval Ordnance Development Unit Johns Hopkins University Radiation Laboratory Homewood Campus Baltimore 18, Maryland Attention: Dr. C. R. Larkin
1	Applied Physics Laboratory Johns Hopkins University 8621 Georgia Avenue Silver Spring, Maryland

6	Library of Congress Navy Research Section Washington, D. C.
1	Massachusetts Institute of Technology Research Laboratory of Electronics Cambridge, Massachusetts Attention: Professor L. J. Chu
1	Stanford University Stanford, California Attention: Professor K. Spangenberg
1	University of Illinois Urbana, Illinois Attention: Professor E. C. Jordan
1	Ohio State University Columbus, Ohio Attention: Dr. V. H. Rumsey
1	Cornell University Ithaca, New York Attention: Professor C. R. Burrows
1	University of California Berkeley, California Attention: Electrical Engineering Department
1	Oregon State College Corvallis, Oregon Attention: Professor J. J. Brady
1	University of Texas Austin, Texas Attention: Electrical Engineering Department

* * *

50	Signal Corps, Transportation Officer Asbury Park New Jersey
50	Chief, Administration Section Electronics Research Division Air Force Cambridge Research Center Cambridge, Massachusetts
1	Signal Corps Liaison Office Massachusetts Institute of Technology Attention: Mr. R. E. Campbell

2 National Bureau of Standards
Washington, D. C.
Attention: Librarian

1 Document Room
Research Laboratory of Electronics
Massachusetts Institute of Technology
Attention: Mr. Hewitt

1 Library
Watson Laboratories
Red Bank, New Jersey